5 Fibre Bragg Gratings

Andreas Othonos, Kyriacos Kalli, David Pureur and Alain Mugnier

5.1 Introduction

The discovery of fibre optics has revolutionized the field of telecommunications making possible high-quality, high-capacity, long distance telephone links. Over the past three decades the advancements in optical fibre have undoubtedly improved and reshaped fibre optic technology so that optical fibres plus related components have become synonymous with "telecommunication". In addition to applications in telecommunications, optical fibres are also utilized in the rapidly growing field of fibre sensors. Despite the improvements in optical fibre manufacturing and advancements in the field in general, it has remained challenging to integrate basic optical components such as mirrors, wavelength filters, and partial reflectors with fibre optics. Recently, however, all this has changed with the ability to alter the core index of refraction in a single-mode optical fibre by optical absorption of UV light. The photosensitivity of optical fibres allows the fabrication of phase structures directly into the fibre core, called *fibre Bragg gratings* (FBG), Fig. 5.1. Photosensitivity refers to a permanent change in the index of refraction of the fibre core when exposed to light with characteristic wavelength and intensity that depend on the core material. The fibre Bragg grating can perform many primary functions, such as reflection and filtering for example, in a highly efficient, low loss manner. This versatility has stimulated a number of significant innovations [1–3].

For a conventional fibre Bragg grating the periodicity of the index modulation has a physical spacing that is one half of the wavelength of light propagating in the waveguide (phase matching between the grating planes and incident light results in coherent back reflection). Reflectivities approaching 100% are possible, with the grating bandwidth tailored from typically 0.1 nm to more than tens of nanometres. These characteristics make Bragg gratings suitable for telecommunications, where they are used to reflect, filter or disperse light [1]. Fibre lasers capable of producing light at telecommunications windows utilize Bragg gratings for forming both, the high-reflectivity end mirror and output coupler to the laser cavity, resulting

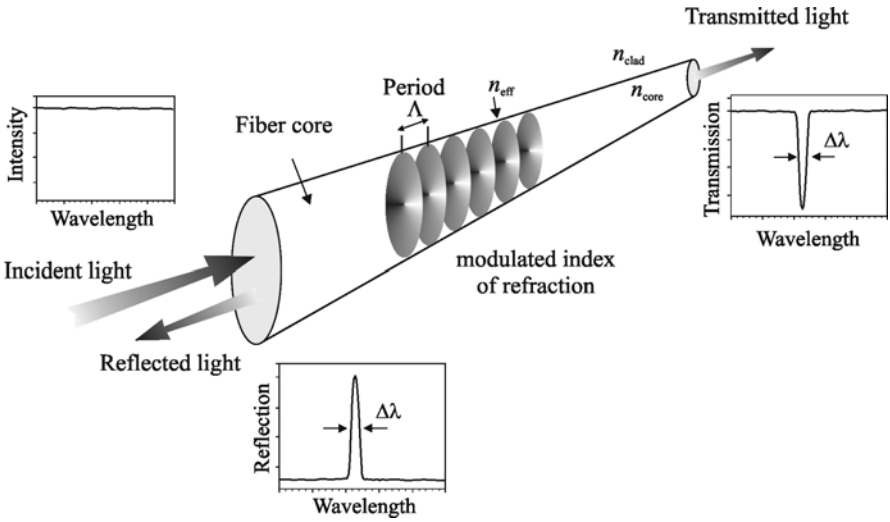

Fig. 5.1. Schematic representation of a Bragg grating inscribed into the core of an optical fibre. The period of the index of refraction variation is represented by Λ. A broadband light is coupled into the core of the fibre. Part of the input light is reflected (at the Bragg condition) and the rest is transmitted. The bandwidth of the reflected and transmitted light depends on the characteristics of the Bragg grating, its length and modulation depth

in an efficient and inherently stable source. Moreover, the ability of gratings with non-uniform periodicity to compress or expand pulses is particularly important to high-bit-rate, long-haul communication systems. Grating-based tuneable dispersion compensator devices can be used to alleviate non-linear signal distortion resulting from optical power variations. A multitude of grating-based transmission experiments has been reported [4], including 10 Gbit/s over 400 km of non-dispersion-shifted fibre with fixed dispersion compensation using chirped fibre Bragg gratings [5]. Power penalties are routinely less than 1 dB [6, 7]. In optical systems with bit rates of 40 Gbit/s and higher, tuneable dispersion compensation becomes necessary to maintain system performance. Tuneable chirp devices through uniform tuning of nonlinearly chirped Bragg gratings [8], or a non-uniform gradient via temperature [9] or strain gradients [10–12] along the grating length have been demonstrated. Systems employing Bragg gratings have demonstrated in excess of 100 km–40 Gbit/s transmission [4]. Given that future systems will operate at bit rates of 160 Gbit/s accurate dispersion maps are required for the fibre network, furthermore at this bit rate there are no electronic alternatives and dispersion compensation must be all-optical and tuneable in nature. There are demonstrations to 100 km at this repetition rate using tuneable, chirped gratings [13]. Furthermore, the Bragg grating meets the demands of

dense wavelength division multiplexing, which requires narrowband, wavelength-selective components, offering very high extinction between different information channels. Numerous applications exist for such low loss, fibre optic filters, examples of which are ASE noise suppression in amplified systems, pump recycling in fibre amplifiers, and soliton pulse control.

The grating planes are subject to temperature and strain perturbations, as is the host glass material, modifying the phase matching condition and leading to wavelength dependent reflectivity. Typically, at 1.5 μm, the wavelength-strain responsivity is ~1 pm/με, with a wavelength shift of about 10 to 15 pm/°C for temperature excursions (strain ε defined as Δ-length/length). Therefore by tracking the wavelength at which the Bragg reflection occurs the magnitude of an external perturbation may be obtained. This functionality approaches the ideal goal of optical fibre sensors: to have an intrinsic in-line, fibre-core structure that offers an absolute readout mechanism. The reliable detection of sensor signals is critical and spectrally encoded information is potentially the simplest approach, offering simple decoding that may even be facilitated by another grating. An alternative approach is to use the grating as a reflective marker, mapping out lengths of optical fibre. Optical time domain measurements allow for accurate length or strain monitoring.

The grating may be photo-imprinted into the fibre core during the fibre manufacturing process, with no measurable loss to the mechanical strength of the host material. This makes it possible to place a large number of Bragg gratings at predetermined locations into the optical fibre to realize a quasi-distributed sensor network for structural monitoring, with relative ease and low cost. Importantly, the basic instrumentation applicable to conventional optical fibre sensor arrays may also incorporate grating sensors, permitting the combination of both sensor types. Bragg gratings are ideal candidates for sensors, measuring dynamic strain to nε-resolution in aerospace applications and as temperature sensors for medical applications. They also operate well in hostile environments such as high pressure, borehole-drilling applications, principally as a result of the properties of host glass material.

Fibre optic photosensitivity has indeed opened a new era in the field of fibre optic based devices [1], with innovative new Bragg grating structures finding their way into telecommunication and sensor applications. Devices like fibre *Fabry–Perot Bragg gratings* for band-pass filters, *chirped gratings* for dispersion compensation and pulse shaping in ultra-short work, and *blazed gratings* for mode converters are becoming routine applications. Fibre optics sensing is an area that has embraced Bragg gratings since the early days of their discovery, and most fibre optics sensor systems today make use of Bragg grating technology.

Within a few years from the initial development, fibre Bragg gratings have moved from laboratory interest and curiosity to implementation in optical communication and sensor systems. In a few years, it may be as difficult to think of fibre optic systems without fibre Bragg gratings as it is to think of bulk optics without the familiar laboratory mirror.

5.2 Fundamentals of Fibre Bragg Gratings

In this section we will describe in detail the various properties that are characteristic of fibre Bragg gratings and this will involve the discussion of a diverse range of topics. We will begin by examining the measurable wavelength-dependent properties, such as the reflection and transmission spectral profiles, for a number of simple and complex grating structures. The dependence of the grating wavelength response to externally applied perturbations, such as temperature and strain, is also investigated.

5.2.1 Simple Bragg Grating

A fibre Bragg grating consists of a periodic modulation of the refractive index in the core of a single-mode optical fibre. These types of uniform fibre gratings, where the phase fronts are perpendicular to the fibre's longitudinal axis with grating planes having constant period (Fig. 5.2), are

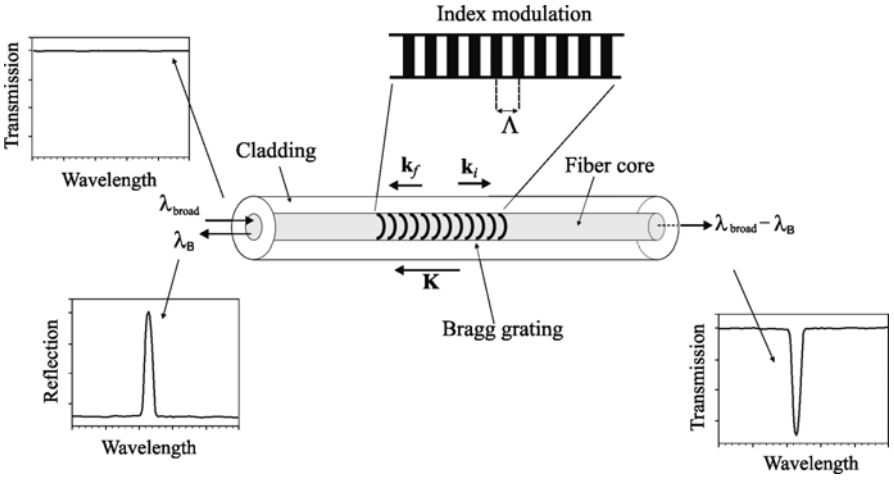

Fig. 5.2. Illustration of a uniform Bragg grating with constant index of modulation amplitude and period. Also shown are the incident, diffracted, and grating wave vectors that have to be matched for momentum conservation

considered the fundamental building blocks for most Bragg grating structures. Light guided along the core of an optical fibre will be scattered by each grating plane. If the Bragg condition is not satisfied, the reflected light from each of the subsequent planes becomes progressively out of phase and will eventually cancel out. Additionally, light that is not coincident with the Bragg wavelength resonance will experience very weak reflection at each of the grating planes because of the index mismatch; this reflection accumulates over the length of the grating. As an example, a 1 mm grating at 1.5 μm with a strong Δn of 10^{-3} will reflect ~0.05% of the off-resonance incident light at wavelengths sufficiently far from the Bragg wavelength. Where the Bragg condition is satisfied the contributions of reflected light from each grating plane add constructively in the backward direction to form a back-reflected peak with a centre wavelength defined by the grating parameters.

The Bragg grating condition is simply the requirement that satisfies both energy and momentum conservation. Energy conservation ($\hbar\omega_f = \hbar\omega_i$) requires that the frequency of the incident and the reflected radiation is the same. Momentum conservation requires that the wavevector of the incident wave, $\boldsymbol{k}_i$, plus the grating wavevector, $\boldsymbol{K}$, equal the wavevector of the scattered radiation $\boldsymbol{k}_f$, which is simply stated as

$$\boldsymbol{k}_i + \boldsymbol{K} = \boldsymbol{k}_f \tag{5.1}$$

where the grating wavevector, $\boldsymbol{K}$, has a direction normal to the grating planes with a magnitude $2\pi/\Lambda$ (Λ is the grating spacing shown in Fig. 5.2). The diffracted wavevector is equal in magnitude, but opposite in direction, to the incident wavevector. Hence the momentum conservation condition becomes

$$2\left(\frac{2\pi n_{eff}}{\lambda_B}\right) = \frac{2\pi}{\Lambda} \tag{5.2}$$

which simplifies to the first order Bragg condition

$$\lambda_B = 2n_{eff}\Lambda \tag{5.3}$$

where the Bragg grating wavelength, λ_B, is the free space centre wavelength of the input light that will be back-reflected from the Bragg grating, and n_{eff} is the effective refractive index of the fibre core at the free space centre wavelength.

5.2.2 Uniform Bragg Grating

Consider a uniform Bragg grating formed within the core of an optical fibre with an average refractive index n_0. The index of the refractive profile can be expressed as

$$n(z) = n_0 + \Delta n \cos\left(\frac{2\pi z}{\Lambda}\right) \tag{5.4}$$

where Δn is the amplitude of the induced refractive index perturbation (typically 10^{-5} to 10^{-3}) and z is the distance along the fibre longitudinal axis. Using coupled-mode theory [14] the reflectivity of a grating with constant modulation amplitude and period is given by the following expression

$$R(l,\lambda) = \frac{\kappa^2 \sinh^2(sl)}{\Delta\beta^2 \sinh^2(sl) + s^2 \cosh^2(sl)} \tag{5.5}$$

where $R(l, \lambda)$ is the reflectivity, which is a function of the grating length l and wavelength λ. κ is the coupling coefficient, $\Delta\beta = \beta - \pi/\Lambda$ is the detuning wavevector, $\beta = 2\pi n_0/\lambda$ is the propagation constant and finally $s^2 = \kappa^2 - \Delta\beta^2$. For sinusoidal variations of the index perturbation the coupling coefficient, κ, is given by

$$\kappa = \frac{\pi \Delta n}{\lambda} M_{power} \tag{5.6}$$

where M_{power} is the fraction of the fibre mode power contained by the fibre core. In the case where the grating is uniformly written through the core, M_{power} can be approximated by $1 - V^{-2}$, where V is the normalized frequency of the fibre, given by

$$V = (2\pi/\lambda) a \sqrt{n_{co}^2 - n_{cl}^2} \tag{5.7}$$

where a is the core radius, and n_{co} and n_{cl} are the core and cladding indices, respectively. At the centre wavelength of the Bragg grating the wavevector detuning is $\Delta\beta = 0$, therefore the expression for the reflectivity becomes

$$R(l,\lambda) = \tanh^2(\kappa l) \tag{5.8}$$

The reflectivity increases as the induced index of refraction change gets larger. Similarly, as the length of the grating increases, so does the resultant reflectivity. Figure 5.3 shows a calculated reflection spectrum as a function of wavelength of a uniform Bragg grating. The side lobes of the resonance are due to multiple reflections to and from opposite ends of the grating region. The sinc spectrum arises mathematically through the

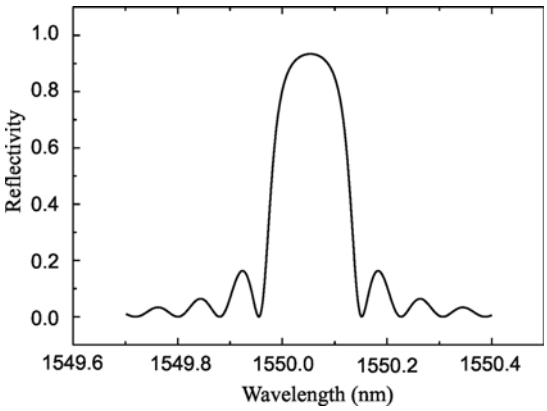

Fig. 5.3. Typical wavelength-dependent reflection spectrum of a Bragg grating with centre wavelength around 1550 nm

Fourier transform of a harmonic signal having finite extent, while an infinitely long grating would transform to an ideal delta function response in the wavelength domain.

A general expression for the approximate full-width-half maximum bandwidth of a grating is given by [15]

$$\Delta\lambda = \lambda_B S \sqrt{\left(\frac{\Delta n}{2n_0}\right)^2 + \left(\frac{1}{N}\right)^2} \tag{5.9}$$

where N is the number of grating planes. For strong gratings (with near 100% reflection) $S \approx 1$ holds, while $S \approx 0.5$ for weak gratings.

5.2.3 Phase and Group Delay of Uniform Gratings

Figure 5.4 shows the phase response of two uniform-period Bragg gratings (λ_B around 1550 nm) as a function of wavelength. The two gratings have the same length (1 cm), however, they have different index perturbation change, namely a "strong" grating with $\delta n_{eff} = 3 \times 10^{-4}$ and a "weak" grating with $\delta n_{eff} = 5 \times 10^{-5}$. It appears that the phase change around the Bragg wavelength decreases with higher index of refraction perturbation.

The group delay of the same two gratings is shown in Fig. 5.5. Strong dispersion (change of group delay with wavelength) is clearly seen at the edge of the stop band and it increases with increasing index perturbation change, although it is limited to a small bandwidth. The group delay is minimum at the centre of the band (see also Chap. 2).

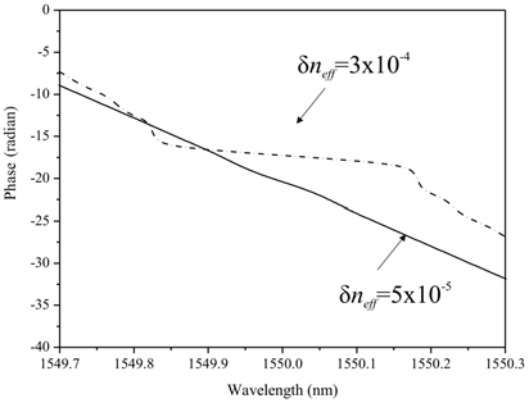

Fig. 5.4. Typical phase response in reflection from a uniform-period Bragg grating as a function of wavelength. The strong grating ($\delta n_{eff} = 3 \times 10^{-4}$) has almost constant phase change in contrast to the characteristics of the weaker grating ($\delta n_{eff} = 5 \times 10^{-5}$)

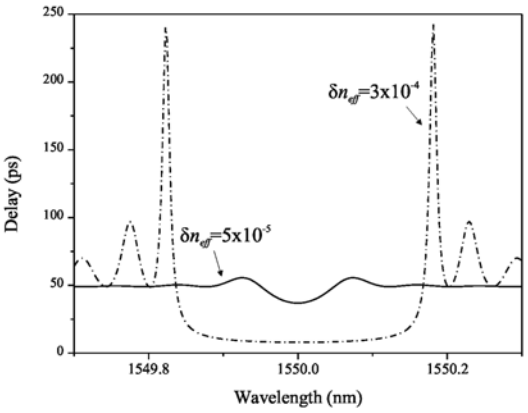

Fig. 5.5. Typical group delay response in reflection from a uniform-period Bragg grating as a function of wavelength. For the strong grating the group delay in the centre of the band is constant, while it increases rapidly at the band edges with increasing bandwidth confinement

5.2.4 Strain and Temperature Sensitivity of Bragg Gratings

The Bragg grating resonance, which is the centre wavelength of back-reflected light from a Bragg grating, depends on the effective index of refraction of the core and the periodicity of the grating. The effective index of refraction, as well as the periodic spacing between the grating planes, will be affected by changes in strain and temperature. Using (5.3) the shift

in the Bragg grating centre wavelength due to strain and temperature changes is given by

$$\Delta\lambda_B = 2\left[\Lambda\frac{\partial n_{eff}}{\partial l} + n_{eff}\frac{\partial \Lambda}{\partial l}\right]\Delta l + 2\left[\Lambda\frac{\partial n_{eff}}{\partial T} + n_{eff}\frac{\partial \Lambda}{\partial T}\right]\Delta T \quad (5.10)$$

The first term in (5.10) represents the strain effect on an optical fibre. This corresponds to a change in the grating spacing and the strain-optic induced change in the refractive index. The above strain effect term may be expressed as [16]

$$\Delta\lambda_B = \lambda_B\left[1 - \frac{n^2}{2}\left[p_{12} - \nu\left(p_{11} + p_{12}\right)\right]\right]\varepsilon_z \quad (5.11)$$

where p_{11} and p_{12} are components of the strain optic tensor, ν is the Poisson's ratio and $\varepsilon_z = \delta l/l$. A typical germanosilicate fibre exhibits a 1.2 pm shift in the centre wavelength of the grating as a result of applying 1 με to the Bragg grating. Experimental results of a Bragg centre wavelength shift with applied stress on a 1555.1 nm grating are shown in Fig. 5.6.

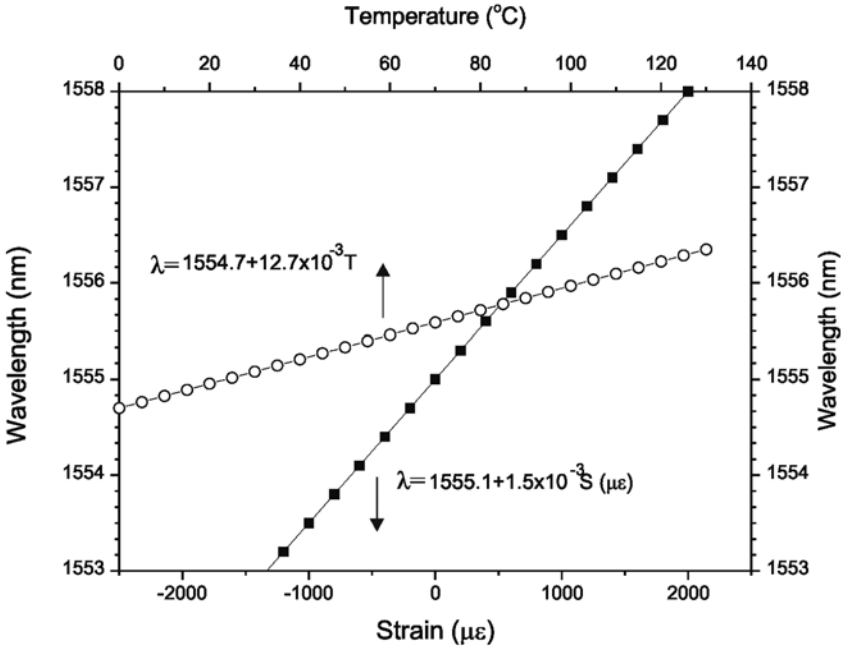

Fig. 5.6. Peak reflection from a Bragg grating under applied strain (*square symbols*) and at different temperatures (*open circles*). The Bragg grating formed the output coupler of an erbium-doped fibre laser

The second term in (5.10) represents the effect of temperature on an optical fibre. A shift in the Bragg wavelength due to thermal expansion changes the grating spacing and the index of refraction. This fractional wavelength shift for a temperature change ΔT may be written as [16]

$$\Delta\lambda_B = \lambda_B \left(\alpha_\Lambda + \alpha_n\right)\Delta T \tag{5.12}$$

where $\alpha_\Lambda = (1/\Lambda)(\partial\Lambda/\partial T)$ is the thermal expansion coefficient for the fibre (approximately 0.55×10^{-6} for silica). The quantity $\alpha_n = (1/n)(\partial n/\partial T)$ represents the thermo-optic coefficient and its approximately equal to 8.6×10^{-6} for a germanium-doped, silica-core fibre. Clearly the index change is by far the dominant effect. From (5.12) the expected sensitivity for a ~1550 nm Bragg grating is approximately 14 pm/°C, in close agreement with the data shown in Fig. 5.6, which illustrate results of a Bragg grating centre wavelength shift as a function of temperature. It is apparent that any change in wavelength, associated with the action of an external perturbation to the grating, is the sum of strain and temperature terms. Therefore, in sensing applications where only one perturbation is of interest, the deconvolution of temperature and strain becomes necessary.

5.2.5 Other Properties of Fibre Gratings

When a grating is formed under conditions for which the modulated index change is saturated under UV exposure, then the effective length will be reduced as the transmitted signal is depleted by reflection. As a result, the spectrum will broaden appreciably and depart from a symmetric sinc or Gaussian shape spectrum, whose width is inversely proportional to the grating length. This is illustrated in Figs. 5.7 (a) and (b). In addition, the cosine-like shape of the grating will change into a waveform with steeper sides, and second-order Bragg lines (Fig. 5.7(c)) will appear due to the new harmonics in the Fourier spatial spectrum of the grating [17].

The presence of higher order grating modes has been utilised as a means of separating temperature and strain measurements using a single grating device, as the grating response to external perturbations is wavelength dependent [18]. Another interesting feature, which is observed in strongly reflecting gratings with large index perturbations, is the small-shape spectral resonance on the short wavelength side of the grating centre line. This is due to self-chirping from $\Delta n_{eff}(z)$. Such features do not occur if the average index change is held constant or adjusted to be constant by a second exposure of the grating. A Bragg grating will also couple dissimilar modes in reflection and transmission, provided the following two conditions are

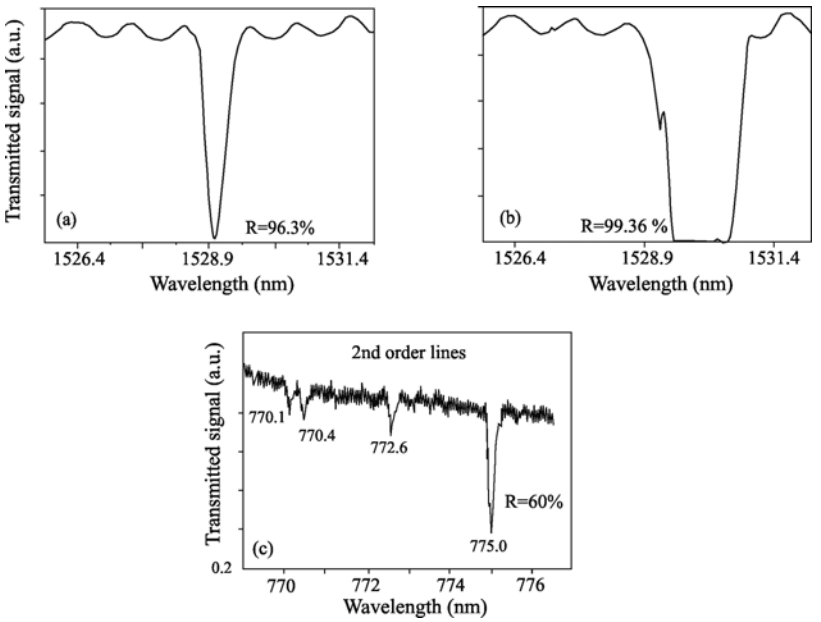

Fig. 5.7. Transmission of standard Bragg grating (**a**) and of Bragg grating with large index change due to saturation under UV exposure (**b**). The spectrum (**b**) broadens under continuous exposure because the incident wave is completely reflected before reaching the end of the grating. The strongly saturated grating is no longer sinusoidal, and the peak index regions are flattened, whereas the valleys in the perturbation index distribution are sharpened. As a result second order Bragg reflection lines (**c**) are observed at about one-half the fundamental Bragg wavelength and at other shorter wavelengths for higher order modes (after [17])

satisfied, namely phase matching and sufficient mode overlap in the region of the fibre that contains the grating. The phase matching condition, which ensures a coherent exchange of energy between the modes, is given by [17]

$$n_{eff} - \frac{\lambda}{\Lambda_z} = n_e \tag{5.13}$$

where n_{eff} is the modal index of the incident wave and n_e is the modal index of the grating-coupled reflected or transmitted wave. It should be pointed out that the above equation allows for a tilted or blazed grating by adjusting the grating pitch along the fibre axis Λ_z.

Normally Bragg gratings do not only reflect radiation into back-travelling guided modes, but also into cladding and radiation modes at wavelengths shorter than the Bragg wavelength. Since these modes are not guided, they are not observed in reflection, but in transmission only.

A schematic illustration of the combined effect of cladding and radiation mode coupling is given in Fig. 5.8.

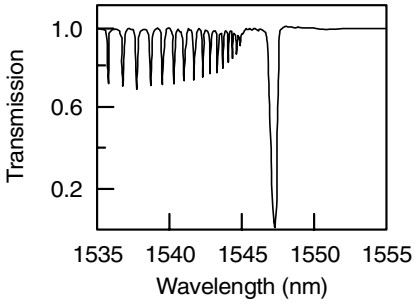

Fig. 5.8. Transmission of strong fibre Bragg grating (schematic) showing loss to radiation modes plus sharp lines due to coupling to distinct cladding modes

Such extra short-wavelength transmission structures are particularly pronounced in highly photosensitive fibres or in hydrogenated ones. In general these losses are unwanted and different methods have been developed in order to suppress them. One approach relies on having a uniform photosensitive region all over the cross-section plane of the optical fibre [19], an alternative variant is the use of fibres with high numerical aperture. For more details including specific references see [1].

5.2.6 Bragg Grating Types

Bragg gratings grow differently in response to particular inscription conditions and the laser used, in addition to the optical fibre type and photosensitivity conditioning prior to inscription. The gratings are characterized by four distinct dynamical regimes known as Type I, Type IA, Type IIA, and Type II. The key differences are highlighted below, bearing in mind that the mechanisms responsible for these types are different. The physical properties of these grating types can be inferred through their growth dynamics and by measurement of thermally induced decay. Broadly speaking Type IA are the least and Type II the most stable gratings with increasing temperature. This is not surprising given that Type IA appears to be a true colour centre grating and purely related to local electronic defects, Type I has both a colour centre and densification element, Type IIA is related to compaction, and Type II is related to fusion of the glass matrix.

Type I Fibre Bragg Gratings

Type I Bragg gratings refer to gratings that are formed in normal photosensitive fibres under moderate intensities. The growth dynamics of the Type I grating is characterized by a power law with time of the form $\Delta n \propto t^{\alpha}$ [20]. It is interesting to point out that the reflection spectra of the guided mode are complementary to the transmission signal, implying that there is negligible loss due to absorption or reflection into the cladding. This is a fundamental characteristic of a Type I Bragg grating. Furthermore, due to the photosensitivity type of the Bragg grating, the grating itself has a characteristic behaviour with respect to temperature erasure. Type I gratings can be erased at relatively low temperatures, approximately 200°C. Nevertheless, Type I gratings are the most utilized Bragg gratings and operate effectively from −40 to +80°C, a temperature range that satisfactorily covers most telecommunications and some sensor applications.

Type IA Fibre Bragg Gratings

Type IA fibre Bragg gratings are the most recently revealed grating type and may be considered a subtype of Type I gratings. (The transmission and reflection spectra are complementary, thus this grating type is indistinguishable from Type I in a static situation.) They are typically formed after prolonged UV exposure of a standard grating in hydrogenated germanosilicate fibre [21, 22], although recent improvements in their inscription have shown that they can be readily inscribed in a suitably prepared optical fibre [23]. The spectral characteristics of Type IA gratings are unique; they are distinct from other grating types as they exhibit a large increase in the mean core index that is identifiable as a large red shift seen in the Bragg wavelength λ_B of the grating during inscription. The mean wavelength change is characterised by three distinct regimes, with the Type I grating growth being superseded by a quasi-linear region followed by saturation. This saturated red shift is dependent on fibre type and hydrogenation conditions, but for a highly doped fibre (either high Ge dopant or B/Ge co-doped fibre) is typically in the order of 15−20 nm, and 5−8 nm for SMF-28 fibre. The maximum wavelength shift translates to an increase in the mean index of up to 2×10^{-2}. More importantly, IA gratings have been shown to exhibit the lowest temperature coefficient of all grating types reported to date, which makes them ideal for use in a temperature compensating, dual grating sensor, as has recently been demonstrated by Kalli and co-workers [24, 25]. Recent studies by Kalli et al. have also shown that their primary limitation of having to work at low temperatures (80°C) can be greatly mitigated if inscribed under strain (stability to 200°C) [26].

Type IIA Fibre Bragg Gratings

Type IIA fibre Bragg gratings appear to have the same spectral characteristics as Type I gratings. The transmission and reflection spectra are again complementary, also rendering this type of grating indistinguishable from Type I in a static situation. However, due to the different mechanism involved in fabricating these gratings, there are some distinguishable features that are noticeable under dynamic conditions either in the initial fabrication or in the temperature erasure of the gratings. Type IIA gratings are inscribed through a long process, following Type I grating inscription [27]. After approximately 30 min of exposure (depending on the fibre type and exposure fluence), the Type IIA grating is fully developed. Clearly, Type IIA gratings are not very practical to fabricate. Although the mechanism of the index change is different from Type I, occurring through compaction of the glass matrix, the behaviour subject to external perturbations is the same for both grating types. Irrespective of the subtleties of the index change on a microscopic scale, the perturbations act macroscopically and, therefore, the wavelength response remains the same. However, when the grating is exposed to high ambient temperature, a noticeable erasure is observed only at temperatures as high as 500°C. A clear advantage of the Type IIA gratings over the Type I is the dramatically improved temperature stability of the grating, which may prove very useful, if the system has to be exposed to high ambient temperatures (as may be the case for sensor applications).

Type II Fibre Bragg Gratings

A single excimer light pulse of fluence $> 0.5\,\mathrm{J/cm^2}$ can photoinduce large refractive-index changes in small, localized regions at the core-cladding boundary, resulting in the formation of the Type II grating [28]. This change results from physical damage through localized fusion that is limited to the fibre core, and it produces very large refractive-index modulations estimated to be close to 10^{-2}. The reflection spectrum is broad and several features appear over the entire spectral profile due to non-uniformities in the excimer beam profile that are strongly magnified by the highly non-linear response mechanism of the glass core. Type II gratings pass wavelengths longer than the Bragg wavelength, whereas shorter wavelengths are strongly coupled into the cladding, as is observed for etched or relief fibre gratings, permitting their use as effective wavelength-selective taps. Results of stability tests have shown Type II gratings to be extremely stable at elevated temperatures [28], surviving temperatures in excess of 800°C for several hours; this superior temperature stability can be utilized for sensing applications in hostile environments.

5.3 Spectral Response from Bragg Gratings

Many models have been developed to describe the behaviour of Bragg gratings in optical fibres [1]. The most widely used technique has been coupled-mode theory, where the counter-propagating fields inside the grating structure, obtained by convenient perturbation of the fields in the unperturbed waveguide, are related by coupled differential equations. Here a simple T-Matrix formalism will be presented for solving the coupled-mode equations for a Bragg grating structure [1] thus obtaining its spectral response.

5.3.1 Coupled-mode Theory and the T-Matrix Formalism

The spectral characteristics of a Bragg grating structure may be simulated using the T-Matrix formalism. For this analysis two counter-propagating plane waves are considered confined to the core of an optical fibre, in which a uniform intra-core Bragg grating of length l and uniform period Λ exists. This is illustrated in Fig. 5.9. The electric fields of the backward- and forward-propagating waves can be expressed as

$$E_a(x,t) = A(x)\exp[\mathrm{i}(\omega t - \beta x)] \qquad \text{and} \qquad (5.14a)$$

$$E_b(x,t) = B(x)\exp[\mathrm{i}(\omega t + \beta x)] \qquad (5.14b)$$

respectively, where β is the wave propagation constant. The complex amplitudes $A(x)$ and $B(x)$ of these electric fields obey the coupled-mode equations [29]

$$\frac{dA(x)}{dx} = \mathrm{i}\kappa B(x)\exp[-\mathrm{i}2(\Delta\beta)x] \qquad (0 \le x \le l) \qquad (5.15a)$$

$$\frac{dB(x)}{dx} = -\mathrm{i}\kappa^* A(x)\exp[\mathrm{i}2(\Delta\beta)x] \qquad (0 \le x \le l) \qquad (5.15b)$$

where $\Delta\beta = \beta - \beta_0$ is the differential propagation constant ($\beta_0 = \pi/\Lambda$, and Λ is the grating period) and κ is the coupling coefficient. For uniform gratings, κ is constant and it is related to the index modulation depth. For a sinusoidally-modulated refractive index the coupling coefficient is real and it is given by (5.6).

Assuming that there are both, forward and backward inputs to the Bragg grating, and boundary conditions $B(0) = B_0$ and $A(l) = A_1$, closed-form solutions for $A(x)$ and $B(x)$ are obtained from (5.15). Following these assumptions, the closed-form solutions for x-dependencies of the two waves are

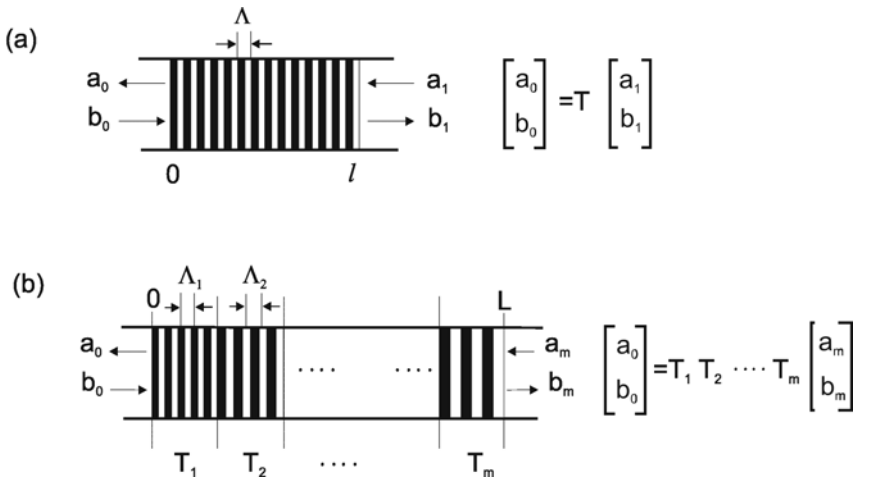

Fig. 5.9. Illustration of T-matrix model: (**a**) single uniform Bragg grating and (**b**) series of gratings with different periods back to back

$a(x) = A(x)\exp(-\mathrm{i}\beta x)$ and $b(x) = B(x)\exp(\mathrm{i}\beta x)$. Therefore, the backward output (reflected wave), a_0, and the forward output (transmitted wave), b_1, from the grating can be expressed by means of the scattering matrix

$$\begin{bmatrix} a_0 \\ b_1 \end{bmatrix} = \begin{bmatrix} S_{11} & S_{12} \\ S_{21} & S_{22} \end{bmatrix} \cdot \begin{bmatrix} a_1 \\ b_0 \end{bmatrix} \tag{5.16}$$

with $a_1 = A_1\exp(\mathrm{i}\beta l)$ and $b_0 = B_0$, and

$$S_{11} = S_{22} = \frac{\mathrm{i}s\exp(-\mathrm{i}\beta_0 l)}{-\Delta\beta\sinh(sl) + \mathrm{i}s\cosh(sl)} \tag{5.17a}$$

$$S_{12} = S_{21}\exp(2\mathrm{i}\beta_0 l) = \frac{\kappa\sinh(sl)}{-\Delta\beta\sinh(sl) + \mathrm{i}s\cosh(sl)} \tag{5.17b}$$

where $s = \sqrt{|\kappa|^2 - \Delta\beta^2}$. Based on the scattering-matrix expression in (5.17), the T-matrix for the Bragg grating is [30]:

$$\begin{bmatrix} a_0 \\ b_0 \end{bmatrix} = \begin{bmatrix} T_{11} & T_{12} \\ T_{21} & T_{22} \end{bmatrix} \cdot \begin{bmatrix} a_1 \\ b_1 \end{bmatrix} \tag{5.18}$$

where

$$T_{11} = T_{22}^{*} = \exp(-\mathrm{i}\beta_0 l)\frac{\Delta\beta \sinh(sl) + \mathrm{i}s\cosh(sl)}{\mathrm{i}s} \tag{5.19a}$$

$$T_{12} = T_{21}^{*} = \exp(-\mathrm{i}\beta_0 l)\frac{\kappa \sinh(sl)}{\mathrm{i}s} \tag{5.19b}$$

The T-matrix relates the input and output of the Bragg grating and is ideal for analyzing a cascade of gratings (Fig. 5.9). Figure 5.9(b) shows a series of gratings back to back with a total length *L*. This grating structure is made up of "*m*" Bragg grating segments. Each segment has a different period Λ_m and has its own T-matrix T_m . The total grating structure may be expressed as

$$\begin{bmatrix} a_0 \\ b_0 \end{bmatrix} = T_1 \cdot T_2 \cdots T_{m-1} \cdot T_m \cdot \begin{bmatrix} a_m \\ b_m \end{bmatrix}, \tag{5.20}$$

and the spectral reflectivity of the grating structure is given by $\left|a_0(\lambda)/b_0(\lambda)\right|^2$. From the phase information one may also obtain the delay for the light reflected back from the grating [1]. It should be noted that this model does not take into account cladding mode-coupling losses.

Grating-length Dependence

The reflection spectral response for uniform Bragg gratings is calculated using the T-matrix formalism described above. The objective of this set of simulations is to demonstrate how the spectral response of a grating is affected as the length of the grating is altered. The index of refraction change is assumed uniform over the grating length, however, the value of the change is reduced with increasing grating length in such a way that the maximum grating reflectivity remains constant. Figure 5.10 shows the spectral profile of three uniform Bragg gratings.

The various plots clearly demonstrate that the bandwidth of the gratings decreases with increasing length. The 1-cm long uniform grating has a bandwidth of approximately 0.15 nm, that of the 2-cm long grating is 0.074 nm and finally the 4-cm long grating exhibits 0.057 nm bandwidth. Theoretically Bragg gratings may be constructed with extremely small bandwidths by simply increasing the grating length. However, in practice such devices are not easy to manufacture. The error associated with the spacing between the periods of a grating (during manufacturing) is cumulative, therefore, with increasing grating length the total error increases, resulting in out-of-phase periods and leading to broadening of the Bragg

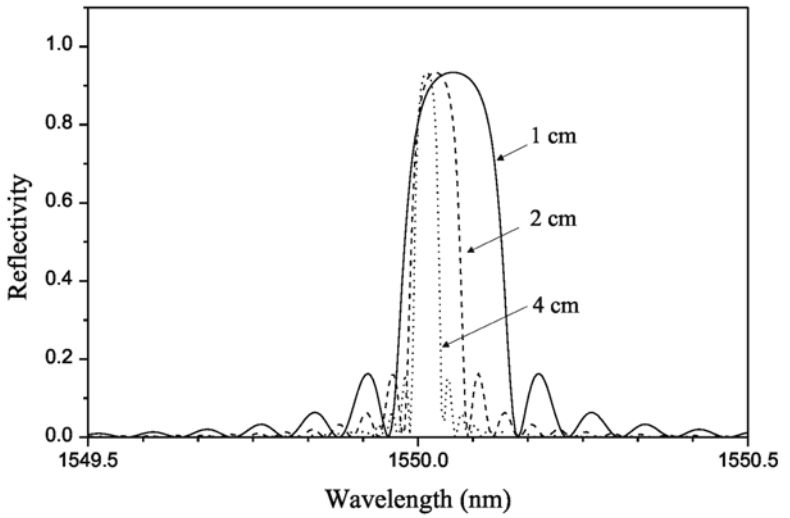

Fig. 5.10. Spectral reflectivity response from uniform Bragg gratings. The various spectral profiles correspond to different grating lengths: 1 cm (*solid-*), 2 cm (*dashed-*), and 4 cm (*dotted curve*)

grating reflection. Furthermore, if a long perfect Bragg grating is constructed, the effects of the environment have to be considered very carefully. For example, any strain or temperature fluctuations on any part of the grating will cause the periods to move out of phase resulting in broadening of the Bragg grating reflection.

Index of Refraction Dependence

Figure 5.11 shows a set of simulations assuming a uniform Bragg grating of 2 cm length and different index of refraction changes. For the first grating with $\Delta n = 0.5 \times 10^{-4}$ the reflectivity is 90% and the bandwidth is approximately 0.074 nm. If the change of the index of refraction is reduced to half the value of the first grating ($\Delta n = 0.25 \times 10^{-4}$), the reflectivity decreases to 59% and the bandwidth to 0.049 nm. A further decrease in the index of refraction change ($\Delta n = 0.1 \times 10^{-4}$) results in a reflectivity of 15% and a bandwidth of 0.039 nm. It appears that the bandwidth approaches a minimum value and remains constant for further reductions in the index of refraction change.

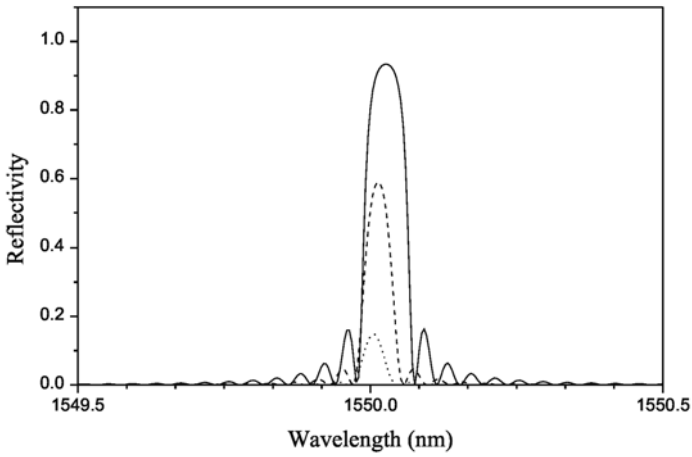

Fig. 5.11. Spectral reflectivity response from uniform Bragg grating 2 cm in length for different refraction indices. The solid, dashed, and dotted lines correspond to $\Delta n = 0.5 \times 10^{-4}$, $\Delta n = 0.25 \times 10^{-4}$, and $\Delta n = 0.1 \times 10^{-4}$ index of refraction change, respectively

Time Delay Dependence

Figure 5.12 shows the delay τ calculated from the derivative of the phase with respect to the wavelength for a uniform grating length L of about 10 mm. The design wavelength for this grating was 1550 nm and the index of refraction of the fibre was set at $n_{eff} = 1.45$. Figure 5.12 also shows the reflectivity spectral response of the same Bragg grating. Clearly both,

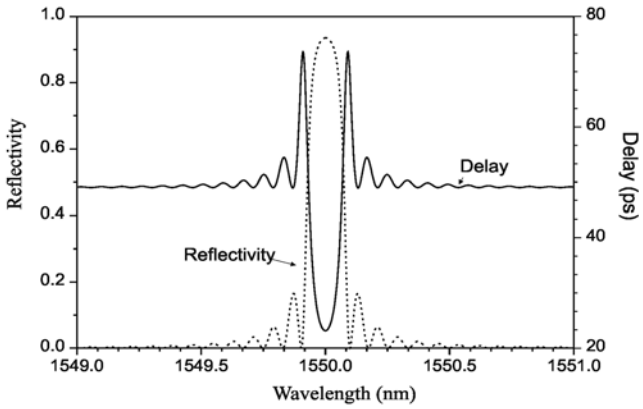

Fig. 5.12. Calculated group delay (*solid line*) and reflectivity (*dotted line*) for uniform weak Bragg grating ($v * \delta n_{eff} = 1 \times 10^{-4}$ and $L = 10$ mm). Design wavelength of the grating: 1550 nm, fringe visibility $v = 100\%$

reflectivity and delay, are symmetric about the peak wavelength λ_{max}. The dispersion is zero near λ_{max} for uniform gratings and becomes appreciable near the band edges and side lobes of the reflection spectrum, where it tends to vary rapidly with wavelength.

5.3.2 Chirped Bragg Gratings

One of the most interesting Bragg grating structures with immediate applications in telecommunications is the chirped Bragg grating. This grating has a monotonically varying period, as illustrated schematically in Fig. 5.13. There are certain characteristic properties offered by monotonically varying the period of gratings that are considered advantages for specific applications in telecommunication and sensor technology, such as dispersion compensation and the stable synthesis of multiple-wavelength sources. These types of gratings can be realized by axially varying either the period of the grating Λ or the index of refraction of the core, or both. From (5.3) we have

$$\lambda_B(z) = 2n_{eff}(z)\Lambda(z) \tag{5.21}$$

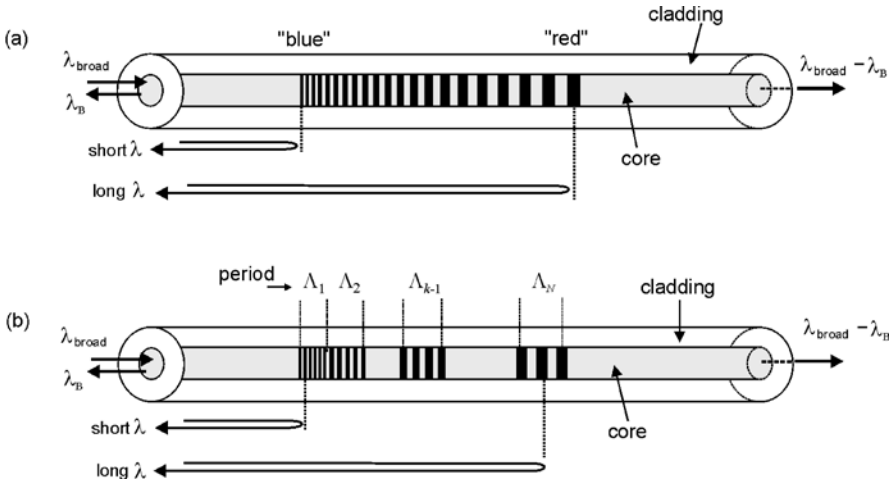

Fig. 5.13. (**a**) Schematic diagram of a chirped grating with an aperiodic pitch. For forward-propagating light as shown, long wavelengths travel further into the grating than shorter wavelengths before being reflected. (**b**) Schematic diagram of a cascade of several gratings with increasing period that are used to simulate long, chirped gratings

The simplest type of chirped grating structure is one with a linear variation of the grating period

$$\Lambda(z) = \Lambda_0 + \Lambda_1 z \tag{5.22}$$

where Λ_0 is the starting period and Λ_1 is the linear change (slope) along the length of the grating. One may consider such a grating structure made up of a series of smaller length uniform Bragg gratings increasing in period. If such a structure is designed properly one may realize a broadband reflector. Typically the linear chirped grating has associated with it a chirp value/unit length ($chirp_\lambda = 2n_0\Lambda_1$) and the starting period. For example, a chirped grating 2 cm in length may have a starting wavelength at 1550 nm and a chirp value of 1 nm/cm. This implies that the end of the chirped grating will have a wavelength period corresponding to 1552 nm.

The simulation results shown in Fig. 5.14 illustrate the characteristics of chirped Bragg grating structures. The three different reflection spectra in the left part of Fig. 5.14 correspond to chirp values 0, 0.2, and 0.4 nm over the entire length of the grating. In these calculations all gratings are assumed to be 10 mm long with a constant index of refraction change $\delta n_{eff} = 1 \times 10^{-4}$. With increasing chirp value the reflectivity response becomes broader and the reflection maximum decreases. In these simulations the chirped gratings are approximated by a number of progressively increasing period gratings, whose total length amounts to the length of the chirped grating. The number of "steps" (the number of smaller gratings) assumed in the calculations is 100 (simulations indicated that calculations

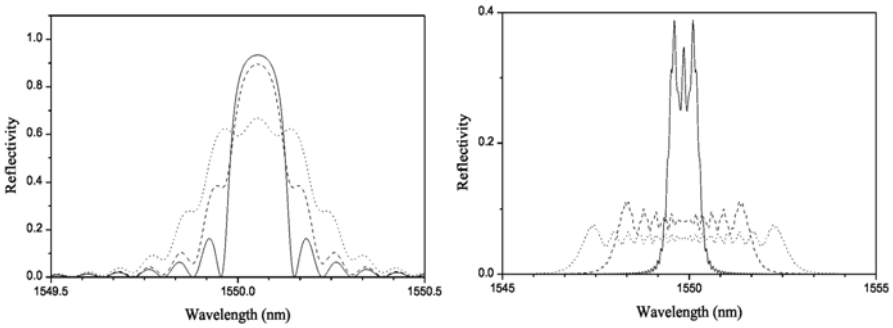

Fig. 5.14. Spectral reflectivity response from different Bragg gratings showing the effect of chirping. All gratings are 10 mm long and the index of refraction change is assumed to be $\delta n_{eff} = 1 \times 10^{-4}$ for all of them. Left part: The solid curve corresponds to 0 chirp, the dashed and dotted curves correspond to 0.2 and 0.4 nm chirp, respectively (where the chirp value is over the length of the grating). Right part: Spectral reflectivity response from highly chirped Bragg gratings for chirp values of 1 nm, 4 nm, and 8 nm over the 10 mm length of the gratings

with more than 20 steps will give approximately the same result). The spectral response from Bragg gratings with very large chirp values (1, 4, and 8 nm over the 10 mm length of the grating) is shown in the right part of Fig. 5.14. As can be seen it is possible to span a very large spectral area with increasing chirp value, however, with a reduction in the maximum reflectivity of the grating. This problem may be overcome by increasing the index of refraction modulation.

5.3.3 Apodisation of Spectral Response of Bragg Gratings

The reflection spectrum of a finite length Bragg grating with uniform modulation of the index of refraction gives rise to a series of side lobes at adjacent wavelengths (cf. Figs. 2.1 (log scale!), 5.3 or 5.12). It is very important to minimize and if possible eliminate the reflectivity of these side lobes, (or apodize the reflection spectrum of the grating) in devices where high rejection of the non-resonant light is required. An additional benefit of apodization is the improvement of the dispersion compensation characteristics of chirped Bragg gratings [31]. In practice apodization is accomplished by varying the amplitude of the coupling coefficient along the length of the grating. One method used to apodize an FBG consists in exposing the optical fibre with the interference pattern formed by two non-uniform ultraviolet light beams [32]. In the phase mask technique, apodization can be achieved by varying the exposure time along the length of the grating, either from a double exposure, by scanning a small writing beam, or by using a variable diffraction efficiency phase mask. In all these apodization techniques, the variation in coupling coefficient along the length of the grating comes from local changes in the intensity of the UV light reaching the fibre.

Figure 5.15 demonstrates the characteristics of apodized Bragg gratings, to be compared for example with Figs. 2.1, 5.3, or 5.12, which illustrate the typical side lobes of uniform Bragg gratings. For both gratings of Fig. 5.15 the magnitude of the index variation and the extension of the apodized regions are the same, but in the first case (left) the average refractive index changes also along the apodized region, while it remains constant for the second example (right part of Fig. 5.15). It is obvious that the latter approach results in a significantly stronger side lobe suppression.

Apodization of the fibre Bragg grating spectral response has been reported by Albert et al. using a phase mask with variable diffraction efficiency [33]. Bragg gratings with side lobe levels 26 dB lower than the peak reflectivity have been fabricated in standard telecommunication fibres [34]. This represents a reduction of 14 dB in the side lobe levels compared to uniform gratings with the same bandwidth and reflectivity.

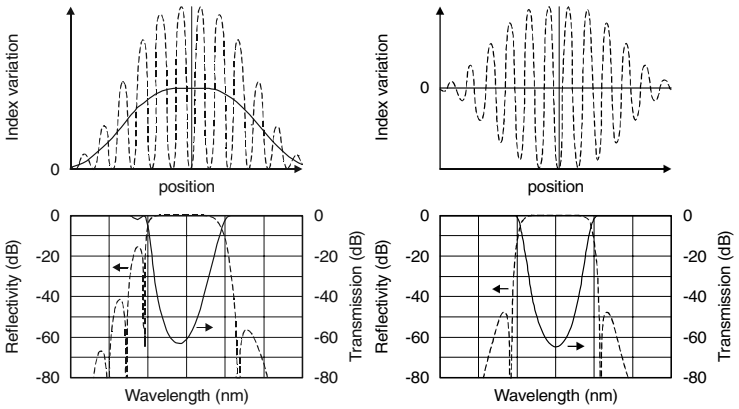

Fig. 5.15. Index variation and corresponding reflectivity and transmission of apodised gratings with varying (*left*) and constant (*right*) average effective refractive index

A technique for cosine apodization that was obtained by repetitive, symmetric longitudinal stretching of the fibre around the centre of the grating while the grating was written has also been demonstrated [35]. This apodization scheme is applicable to all types of fibre gratings, written by direct replication by a scanning or a static beam, or by use of any other interferometer and is independent of length. The simplicity of this technique allows the rapid production of fibre gratings required for wavelength-division-multiplex (WDM) systems and for dispersion compensation.

5.3.4 Fibre Bragg Gratings with Other Types of Mode Coupling

Tilting or blazing the Bragg grating at angles with respect to the fibre axis can couple light out of the fibre core into cladding modes or to radiation modes outside the fibre. This wavelength-selective tapping occurs over a rather broad range of wavelengths that can be controlled by the grating and waveguide design. One of the advantages is that the signals are not reflected into the fibre core, and thus the tap forms an absorption type of filter. An important application is gain flattening filters for erbium-doped fibre amplifiers (cf. Sect. 5.5.5).

With a small tilt of the grating planes to the fibre axis (~1°), one can make a reflecting spatial mode coupler such that the grating reflects one guided mode into another. It is interesting to point out that by making long period gratings, one can perturb the fibre to couple to other forward going modes. A wavelength filter based on this effect has been demonstrated by Hill et al. [36]. The spatial mode-converting grating was written using the point-by-point technique (cf. Sect. 5.4.4) with a period of 590 μm over a length of

60 cm. Using mode strippers before and after the grating makes a wavelength filter. In a similar manner, a polarisation mode converter or rocking filter in polarisation-maintaining fibre can be made. A rocking filter of this type, generated with the point-by-point technique, was also demonstrated by Hill and co-workers [37]. In their work they demonstrated an 87 cm long, 85 step rocking filter that had a bandwidth of 7.6 nm and a peak transmission of 89%.

5.4 Fabrication of Fibre Bragg Gratings

In the following section we will describe various techniques used in fabricating standard and complex Bragg grating structures in optical fibres. Depending on the fabrication technique Bragg gratings may be labelled as internally or externally written. Although internally written Bragg gratings may not be considered very practical or useful, nevertheless it is important to consider them, thus obtaining a complete historical perspective. Externally written Bragg gratings, that is gratings inscribed using techniques such as interferometric, point-by-point, and phase-mask overcome the limitations of internally written gratings and are considered far more useful. Although most of these inscription techniques were initially considered difficult due to the requirements of sub-micron resolution and thus stability, they are well controlled today and the inscription of Bragg gratings using these techniques is considered routine.

5.4.1 Internally Inscribed Bragg Gratings

Internally inscribed Bragg gratings were first demonstrated in 1978 by Hill and co-workers [38, 39] in a simple experimental set-up as shown in Fig. 5.16. An argon ion laser was used as the source, oscillating on a single longitudinal mode at 514.5 nm (or 488 nm) exposing the photosensitive fibre by coupling light into its core. Isolation of the argon ion laser from the back-reflected beam was necessary to avoid instability. Furthermore, the pump laser and the fibre were placed in a tube for thermal isolation. The incident laser light interfered with the 4% reflection (from the cleaved end of the fibre) to initially form a weak standing wave intensity pattern within the core of the fibre. At the high intensity points the index of refraction in the photosensitive fibre changed permanently. Thus a refractive index perturbation having the same spatial periodicity as the interference pattern was formed. These types of gratings normally have a long length (tens of centimetres) in order to achieve useful reflectivity values due to the small index of refraction changes.

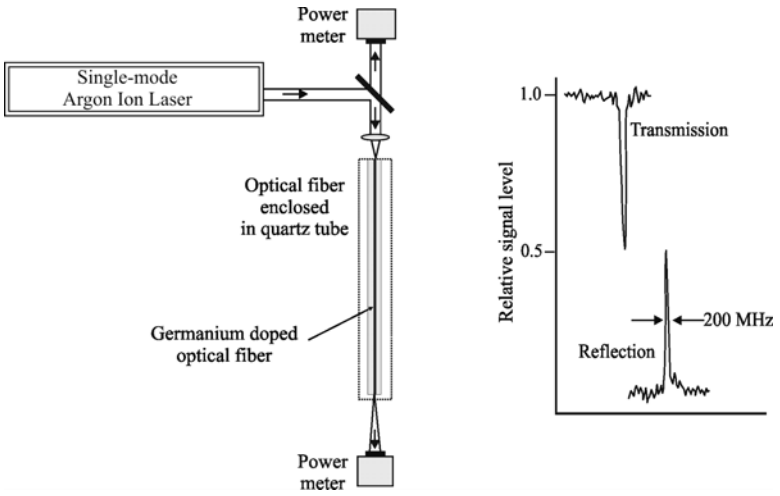

Fig. 5.16. A typical apparatus used in generating self-induced Bragg gratings using an argon ion laser. Typical reflection and transmission characteristics of these types of gratings are shown in the graph

5.4.2 Interferometric Inscription of Bragg Gratings

Amplitude-splitting Interferometer

The interferometric fabrication technique, which is an external writing approach for inscribing Bragg gratings in photosensitive fibres, was first demonstrated by Meltz and coworkers [40], who used an amplitude-splitting interferometer to fabricate fibre Bragg gratings in an experimental arrangement similar to the one shown in Fig. 5.17. An excimer-pumped dye laser operating at a wavelength in the range of 486–500 nm was frequency doubled using a non-linear crystal. This provided a UV source in the 244-nm band with adequate coherence length (a critical parameter in this inscription technique). The UV radiation was split into two beams of equal intensity that were recombined to produce an interference pattern, normal to the fibre axis. A pair of cylindrical lenses focused the light onto the fibre and the resulting focal line was approximately 4-mm long by 124-μm wide. A broadband source was also used in conjunction with a high-resolution monochromator to monitor the reflection and transmission spectra of the grating. The graph in Fig. 5.17 shows the reflection and complementary transmission spectra of the grating formed in a 2.6-μm diameter core, 6.6-mol % GeO_2-doped fibre after 5 minutes exposure to a 244-nm interference pattern with an average power of 18.5 mW. The length of the exposed region was estimated to be between 4.2 and 4.6 mm.

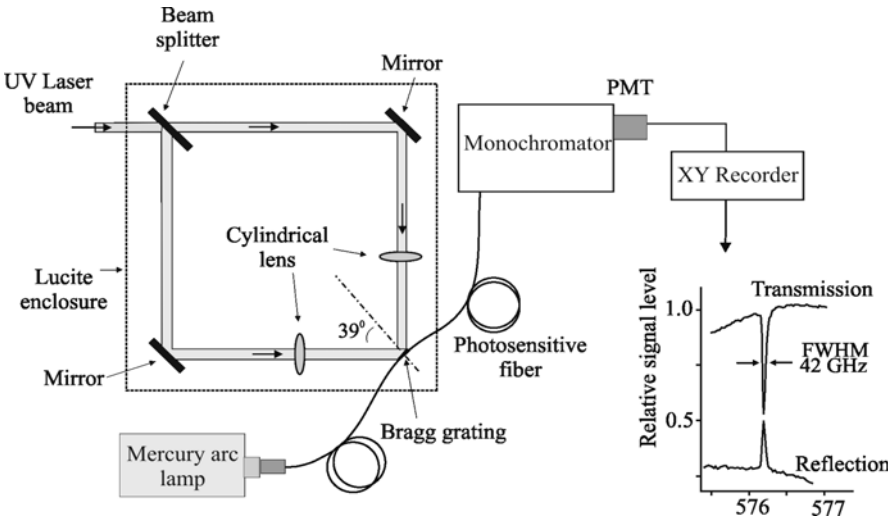

Fig. 5.17. An amplitude-splitting interferometer used by Meltz et al. [40], which demonstrated the first externally fabricated Bragg grating in optical fibre. The reflection and transmission spectra of a 4.4-mm long Bragg grating fabricated with this apparatus are also shown

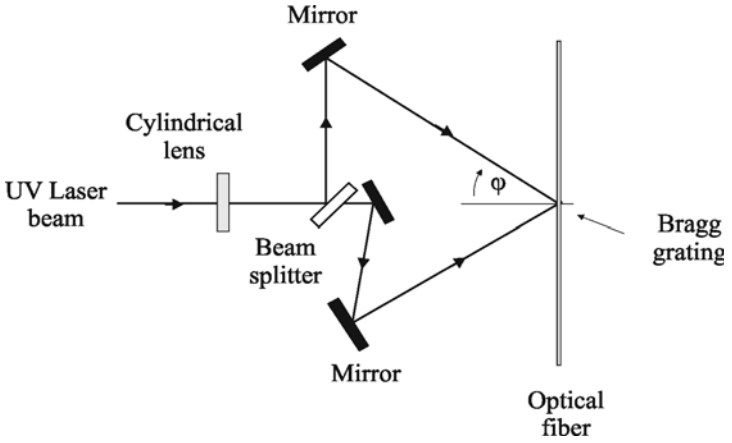

Fig. 5.18. An improved version of the amplitude-splitting interferometer, where an additional mirror is used to achieve an equal number of reflections, thus eliminating the different lateral orientations of the interfering beams. This type of interferometer is applicable to fabrication systems where the source spatial coherence is low, such as with excimer lasers

In a conventional interferometer such as the one shown in Fig. 5.17 the UV writing laser light is split into equal intensity beams that subsequently recombine after having undergone a different number of reflections in each optical path. Therefore, the interfering beams (wave fronts) acquire different (lateral) orientations. This results in a low quality fringe pattern for laser beams having low spatial coherence. This problem is eliminated by including a second mirror in one of the optical paths, as shown in Fig. 5.18, which in effect compensates for the beam splitter reflection. Since the total number of reflections is now the same in both optical arms, the two beams interfering at the fibre are identical.

The interfering beams are normally focused to a fine line matching the fibre core using a cylindrical lens placed outside the interferometer. This results in higher intensities at the core of the fibre, thereby improving the grating inscription. In interferometer systems as the ones shown in Figs. 5.17 and 5.18 the interference fringe pattern period Λ depends on both the irradiation wavelength λ_w and the half angle between the intersecting UV beams φ (cf. Fig. 5.18). Since the Bragg grating period is identical to the period of the interference fringe pattern, the fibre grating period is given by

$$\Lambda = \frac{\lambda_w}{2\sin\varphi}. \tag{5.23}$$

Given the Bragg condition, $\lambda_B = 2n_{eff}\Lambda$, the Bragg resonance wavelength, λ_B, can be represented in terms of the UV writing wavelength and the half angle between intersecting UV beams as

$$\lambda_B = \frac{n_{eff}\lambda_w}{\sin\varphi} \tag{5.24}$$

where n_{eff} is the effective core index. From (5.24) one can easily see that the Bragg grating wavelength can be varied either by changing λ_w [41] and/or φ. The choice of λ_w is limited to the UV photosensitivity region of the fibre; however, there is no restriction for the choice of the angle φ.

One of the advantages of the interferometric method is the ability to introduce optical components within the arms of the interferometer, allowing for the wavefronts of the interfering beams to be modified. In practice, incorporating one or more cylindrical lenses into one or both arms of the interferometer produces chirped gratings with a wide parameter range [2]. The most important advantage offered by the amplitude-splitting interferometric technique is the ability to inscribe Bragg gratings at any wavelength desired. This is accomplished by changing the intersecting angle between the UV

beams. This method also offers complete flexibility for producing gratings of various lengths, which allows the fabrication of wavelength-narrowed or broadened gratings. The main disadvantage of this approach is a susceptibility to mechanical vibrations. Sub-micron displacements in the position of mirrors, the beam splitter, or other optical mounts in the interferometer during UV irradiation will cause the fringe pattern to drift, washing out the grating from the fibre. Furthermore, because the laser light travels long optical distances, air currents, which affect the refractive index locally, can become problematic, degrading the formation of a stable fringe pattern. In addition to the above-mentioned shortcomings, quality gratings can only be produced with a laser source that has good spatial and temporal coherence and excellent wavelength and output power stability.

Wavefront-splitting Interferometers

Wavefront-splitting interferometers are not as popular as the amplitude-splitting interferometers for grating fabrication, however, they offer some useful advantages. Two examples of wavefront-splitting interferometers used to fabricate Bragg gratings in optical fibres are the prism interferometer [42, 43] and the Lloyd interferometer [44]. The experimental set-up for fabricating gratings with the Lloyd interferometer is shown in Fig. 5.19. This interferometer consists of a dielectric mirror, which directs half of the UV beam to a fibre that is perpendicular to the mirror. The writing beam is centred at the intersection of the mirror surface and fibre. The overlap of the direct and the deviated portions of the UV beam creates interference fringes normal to the fibre axis. A cylindrical lens is usually placed in front

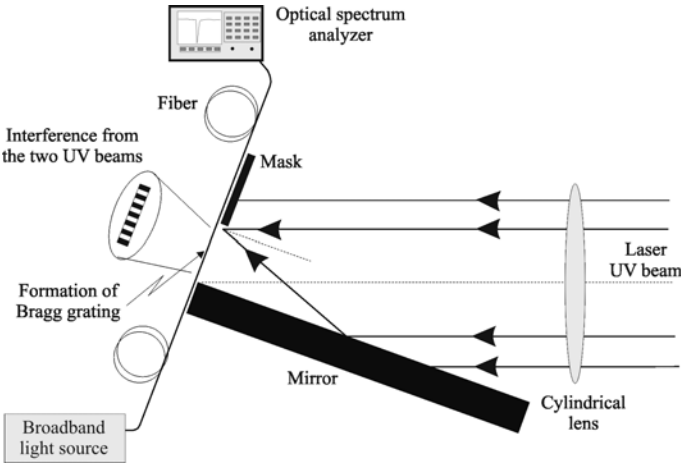

Fig. 5.19. Schematic of the Lloyd wavefront-splitting interferometer

of the system to focus the fringe pattern along the core of the fibre. Since half of the incident beam is reflected, interference fringes appear in a region of length equal to half the width of the beam. Secondly, since half the beam is folded onto the other half, interference occurs, but the fringes may not be of high quality. In the Lloyd arrangement, the folding action of the mirror limits what is possible. It requires a source with a coherence length equal to at least the path difference introduced by the fold in the beam. Ideally the coherence and intensity profile should be constant across the writing beam, otherwise the fringe pattern and thus the inscribed grating will not be uniform. Furthermore, diffraction effects at the edge of the dielectric mirror may also cause problems with the fringe pattern.

A schematic of the prism interferometer is shown in Fig. 5.20. The prism is made from high homogeneity, ultraviolet-grade, fused silica allowing for good transmission characteristics. In this set-up the UV beam is spatially bisected by the prism edge and half the beam is spatially reversed by total internal reflection from the prism face. The two beam halves are then recombined at the output face of the prism, giving a fringe pattern parallel to the photosensitive fibre core. A cylindrical lens placed just before the set-up helps in forming the interference pattern on a line along the fibre core. The interferometer is intrinsically stable as the path difference is generated within the prism and remains unaffected by vibrations. Writing times of over 8 hours have been reported with this type of interferometer. One disadvantage of this system is the geometry of the interference. Folding the beam onto itself forms the interferogram; hence different parts of the beam must interfere, which requires a UV source with good spatial coherence.

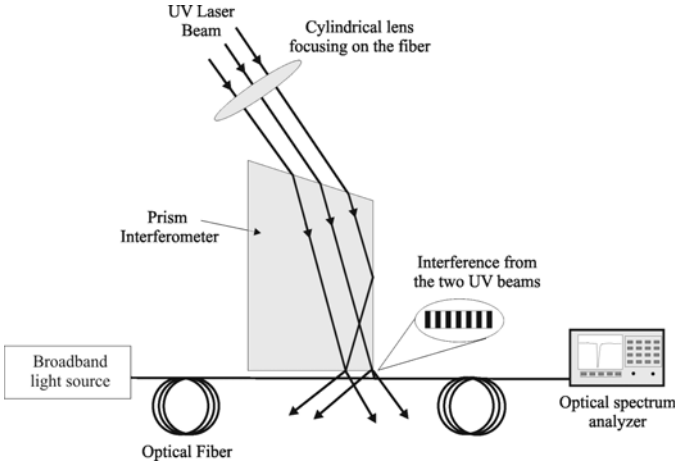

Fig. 5.20. Schematics of the prism wavefront-splitting interferometer

A key advantage of the wavefront-splitting interferometer is the requirement for only one optical component, greatly reducing sensitivity to mechanical vibrations. In addition, the short distance where the UV beams are separated reduces the wavefront distortion induced by air currents and temperature differences between the two interfering beams. Furthermore, this assembly can be easily rotated to vary the angle of intersection of the two beams for wavelength tuning. One disadvantage of this system is the limitation on the grating length, which is restricted to half the beam width. Another disadvantage is the range of Bragg wavelength tuneability, which is restricted by the physical arrangement of the interferometers. As the intersection angle increases, the difference between the beam path lengths increases as well, therefore, the beam coherence length limits the Bragg wavelength tuneability.

Laser Source Requirements

Laser sources used for inscribing Bragg gratings via the above interferometric techniques must have good temporal and spatial coherence. The spatial coherence requirements can be relaxed in the case of the amplitude-splitting interferometer by simply making sure that the total number of reflections are the same in both arms. This is especially critical in the case where a laser with low spatial coherence, like an excimer laser, is used as the source of UV light. The temporal coherence should correspond to a coherence length at least equal to the length of the grating in order for the interfering beams to have a good contrast ratio thus resulting in good quality Bragg gratings. The above coherence requirement together with the UV wavelength range needed (240–250 nm) forced researchers to initially use very complicated laser systems.

One such system consists of an excimer pumped tuneable dye laser, operating in the range of 480 to 500 nm. The output from the dye laser is focused onto a non-linear crystal to double the frequency of the fundamental light (Fig. 5.21). Typically this arrangement provides approximately 3–5 mJ, 10–20 nsec pulses (depending on the excimer pump laser) with excellent temporal and spatial coherence. An alternative to this elaborate and often troublesome set-up is a specially designed excimer laser that has a long temporal coherence length. These spectrally narrow linewidth excimer lasers may operate for extended periods of time on the same gas mixture with little changes in their characteristics. Commercially available narrow linewidth excimer systems are complicated oscillator amplifier configurations, which make them extremely costly. Othonos and Lee [45] developed a low cost simple technique, where existing KrF excimer lasers may be retrofitted with a spectral narrowing system for inscribing Bragg gratings in

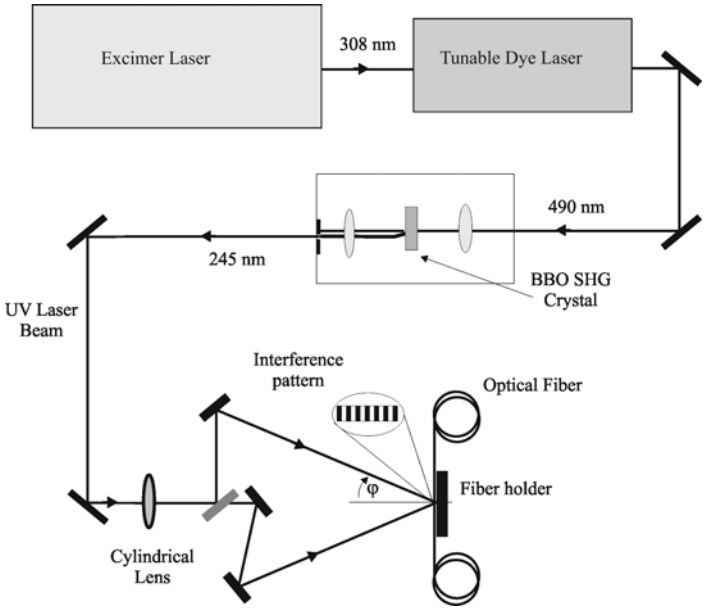

Fig. 5.21. Experimental set-up of an excimer pump dye laser with a frequency-doubled BBO crystal for generating UV light at 245 nm for inscribing Bragg gratings in an interferometer

a side-written interferometric configuration. In that work a commercially available KrF excimer laser (Lumonics Ex-600) was modified to produce a spectrally narrow laser beam (Fig. 5.22) with a linewidth of approximately

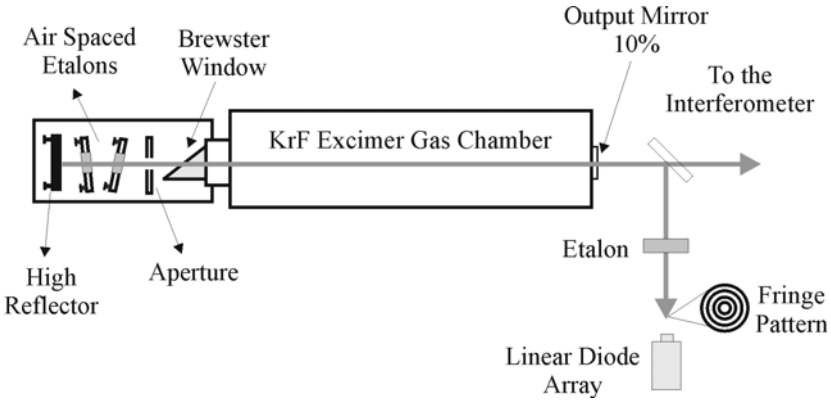

Fig. 5.22. Schematic of a narrow linewidth excimer laser system (KrF) consisting of two air-spaced etalons and an intracavity aperture placed between the KrF excimer gas chamber and the high reflector (after [45])

4×10^{-12} m. This system was used to successfully inscribe Bragg gratings in photosensitive optical fibres [45]. An alternative to the above system, which is becoming very popular, is the intracavity frequency-doubled argon ion laser that uses Beta-Barium Borate (BBO). This system efficiently converts high-power visible laser wavelengths into deep ultraviolet (244 and 248 nm). The characteristics of these lasers include unmatched spatial coherence, narrow linewidth and excellent beam pointing stability, which make such systems very successful in inscribing Bragg gratings in optical fibres [46].

5.4.3 Phase-mask Technique

One of the most effective methods for inscribing Bragg gratings in photosensitive fibre is the phase-mask technique [47]. This method employs a diffractive optical element (phase mask) to spatially modulate the UV writing beam (Fig. 5.23). Phase masks may be formed holographically or by electron-beam lithography. Holographically induced phase masks have no stitch error, which is normally present in the electron-beam phase masks. However, complicated patterns can be written into the electron beam-fabricated masks (quadratic chirps, Moiré patterns etc.). The phase mask grating has a one-dimensional surface-relief structure fabricated in a high quality fused silica flat transparent to the UV writing beam. The

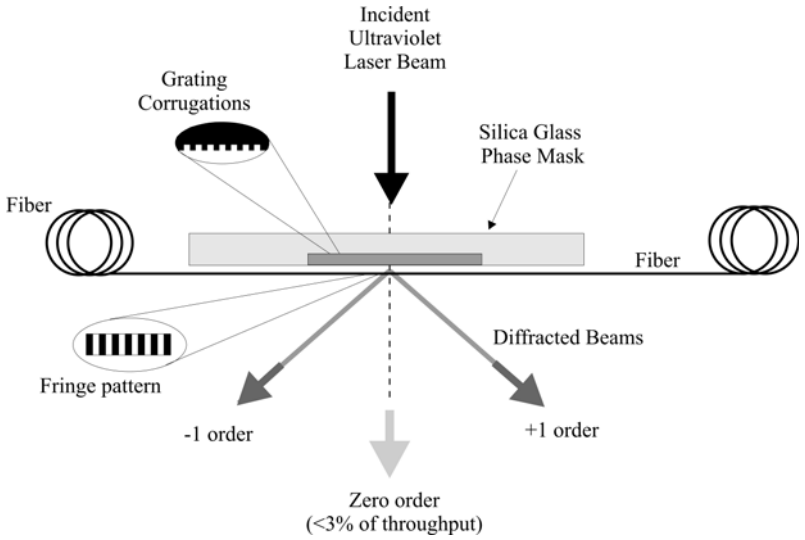

Fig. 5.23. Phase-mask geometry for inscribing Bragg gratings in optical fibres (see also Fig. 5.24)

profile of the periodic surface-relief gratings is chosen such that when a UV beam is incident on the phase mask, the zero-order diffracted beam is suppressed to less than a few percent (typically less than 5%) of the transmitted power. In addition, the diffracted plus and minus first orders are maximized each containing typically more than 35% of the transmitted power. A near field fringe pattern is produced by the interference of the plus and minus first-order diffracted beams. The period of the fringes is one half that of the mask. The interference pattern photo-imprints a refractive index modulation into the core of a photosensitive optical fibre placed in contact with or in close proximity immediately behind the phase mask (Fig. 5.23). A cylindrical lens may be used to focus the fringe pattern along the fibre core.

The phase mask greatly reduces the complexity of the fibre grating fabrication system. The simplicity of using only one optical element provides a robust and inherently stable method for reproducing fibre Bragg gratings. Since the fibre is usually placed directly behind the phase mask in the near field of the diffracting UV beams, sensitivity to mechanical vibrations and therefore stability problems are minimized. Low temporal coherence does not affect the writing capability (as opposed to the interferometric technique) due to the geometry of the problem.

KrF excimer lasers are the most common UV sources used to fabricate Bragg gratings with a phase mask. The UV laser sources typically have low spatial and temporal coherence. The low spatial coherence requires the fibre to be placed in near contact to the grating corrugations on the phase mask in order to induce maximum modulation in the index of refraction. The further the fibre is placed from the phase mask, the lower the induced index modulation, resulting in lower reflectivity Bragg gratings. Clearly, the separation of the fibre from the phase mask is a critical parameter in producing high quality gratings. However, placing the fibre in contact with the fine grating corrugations is not desirable due to possible damage to the phase mask. Othonos and Lee [48] demonstrated the importance of spatial coherence of UV sources used in writing Bragg gratings using the phase-mask technique. Improving the spatial coherence of the UV writing beam does not only improve the strength and quality of the gratings inscribed by the phase-mask technique, it also relaxes the requirement that the fibre has to be in contact with the phase mask.

To understand the significance of spatial coherence in the fabrication of Bragg gratings using the phase-mask technique it is helpful to consider a simple schematic diagram (Fig. 5.24). Consider the fibre core to be at a distance h from the phase mask. The transmitted *plus* and *minus* first orders that interfere to form the fringe pattern on the fibre emanate from different parts of the mask (referred to as distance d in Fig. 5.24). Since the

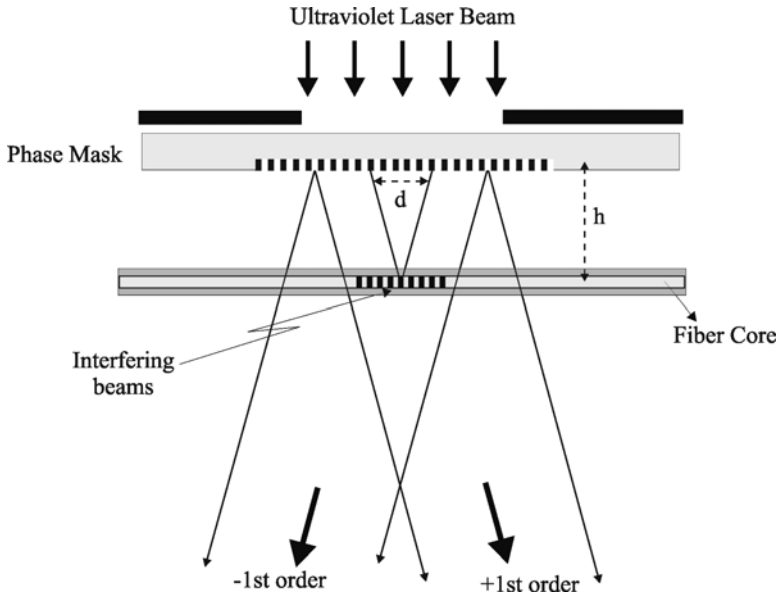

Fig. 5.24. Simple schematic of phase-mask geometry for inscribing Bragg gratings in optical fibres. The plus and minus first-order diffracted beams interfere at the fibre core, placed at distance *h* from the mask

distance of the fibre from the phase mask is identical for the two interfering beams, the requirement for temporal coherence is not critical for the formation of a high contrast fringe pattern. On the other hand, as the distance *h* increases, the separation *d* between the two interfering beams emerging from the mask, increases as well. In this case, the requirement for good spatial coherence is critical for the formation of a high contrast fringe pattern. As the distance *h* extends beyond the spatial coherence of the incident UV beam, the interference fringe contrast will deteriorate, eventually resulting in no interference at all. The importance of spatial coherence was also demonstrated by Dyer et al. [49], who used a KrF laser irradiated phase mask to form gratings in polyimide films. It should also be noted that if the zeroth order beam is not significantly suppressed, interference will occur between 0^{th}- and 1^{st}-order diffracted beams; in this case the interference pattern will change as a function of the fibre-phase mask separation resulting in fringes that vary from half the phase-mask period to one period of the mask.

5.4.4 Point-by-point Fabrication of Bragg Gratings

The point-by-point technique [50] for fabricating Bragg gratings is accomplished by inducing a change in the index of refraction a step at a time

along the core of the fibre. A focused single pulse from an excimer laser produces each grating plane separately. A single pulse of UV light from an excimer laser passes through a mask containing a slit. A focusing lens images the slit onto the core of the optical fibre from the side as shown in Fig. 5.25, and the refractive index of the core increases locally in the irradiated fibre section. The fibre is then translated through a distance Λ corresponding to the grating pitch in a direction parallel to the fibre axis, and the process is repeated to form the grating structure in the fibre core. Essential to the point-by-point fabrication technique is a very stable and precise submicron translational system.

The main advantage of the point-by-point writing technique lies in its flexibility to alter the Bragg grating parameters. Because the grating structure is built up a point at a time, variations in grating length, grating pitch, and spectral response can easily be incorporated. Chirped gratings can be produced accurately simply by increasing the amount of fibre translation each time the fibre is irradiated. The point-by-point method allows the fabrication of spatial mode converters [51] and polarisation mode converters or rocking filters [37], that have grating periods, Λ, ranging from tens of micrometres to tens of millimetres. Because the UV pulse energy can be varied between points of induced index change, the refractive index profile of the grating can be tailored to provide any desired spectral response.

One disadvantage of the point-by-point technique is that it is a tedious process. Because it is a step-by-step procedure, this method requires a relatively long process time. Errors in the grating spacing due to thermal effects and/or small variations in the fibre's strain can occur. This limits

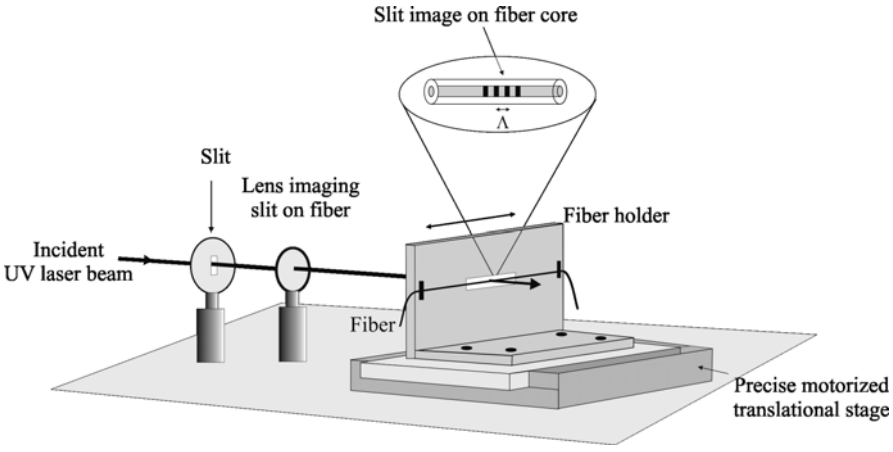

Fig. 5.25. Schematic of set-up for fabricating Bragg gratings using the point-by-point technique

the gratings to very short lengths. Typically, the grating period required for first order reflection at 1550 nm is approximately 530 nm. Because of the submicron translation and tight focusing required, first order 1550 nm Bragg gratings have yet to be demonstrated using the point-by-point technique. Malo et al. [50] have only been able to fabricate Bragg gratings, which reflect light in the 2nd and 3rd order, that have a grating pitch of approximately 1 μm and 1.5 μm, respectively.

5.4.5 Direct-writing Technique

The direct-writing technique [52] is an alternative process for the flexible inscription of high quality gratings in fibre or optical waveguide circuits with integral Bragg gratings. The direct writing-process uses two focused UV laser beams that are overlapped to give a micron-sized, circular spot with an intrinsic linear interference pattern in one dimension, much as a conventional amplitude-splitting interferometer. The interference beam is focused onto the photosensitive fibre or waveguide and translated by one grating period, re-exposed and moved to a new position, systematically building up a grating structure. The piecewise process is where the direct-writing technique differs from the traditional amplitude-splitting arrangement. The sample is moved continuously relative to a modulated laser beam that is synchronised to the sample motion, thereby ensuring a smooth inscription process. Changing the time for which the laser is switched on during the exposure cycle controls the grating contrast. This technique allows for the fabrication of any Bragg grating profile at any point in the structure. The process is computer controlled, providing a straightforward method of producing complex waveguide circuits and Bragg gratings with arbitrary chirp and apodization. Direct writing proves advantageous, as it eliminates the usual need for Bragg grating phase masks. As direct writing is essentially a modified interferometric set-up it has similar limitations regarding system stability requirements.

5.4.6 Femtosecond Laser Inscription of Bragg Gratings

The use of high power femtosecond laser sources for inscribing Bragg gratings has attained significant recent interest. Corresponding laser systems come in myriads of forms: their primary purpose is to produce high-energy laser pulses of 5 to 500 fs duration (150 fs is typical), offering the tempting prospect of extraordinarily high laser intensity when focused onto the sample, 200 GW/cm^2, for example, is not uncommon. The high-energy pulses and wavelength of operation both vary depending on the specific

laser design, and there are, in general, two categories i) oscillator systems without extra optical amplification, where high energy pulses build up in an extended cavity and ii) amplified systems that use external optical amplifiers to enhance oscillator pulse energies. Values of 100 nJ/pulse at 10 MHz repetition rate are typical for extended oscillator cavities; 500 nJ/pulse at 1 MHz have been achieved for cavity-dumped oscillators, and finally 1 mJ/pulse to 10 μJ/pulse for repetition rates of 1 kHz to 500 kHz, respectively, for regeneratively amplified systems. Prior to recent developments, the amplified laser system was economically prohibitive and complex, with separate modules coupled by careful alignment. However, recent developments have seen this scheme replaced by less expensive, diode pumped amplified systems operating in the near infrared that can accept harmonic generators for frequency doubling, tripling, and quadrupling, in a very compact form factor, with minimal infrastructure needs.

The principal advantage of high-energy pulses is their ability of grating inscription in any material type without pre-processing, such as hydrogenation or special core doping with photosensitive materials – the inscription process is controlled multi-photon absorption, void generation and subsequent local refractive index changes. Furthermore, the use of an infrared source or its second harmonic removes the requirement to strip the optical fibre as gratings can readily be written through the buffer layer. However, one must consider that the very nature of the short duration pulse poses several technical difficulties that must be accounted for in choosing a suitable inscription method. Interferometric set-ups must have path lengths matched to within the physical location of the fs pulse; for a 150 fs pulse this corresponds to 45 μm. If a phase mask is utilised the issue of temporal coherence is resolved, but one must now consider the large spectral content of the pulse and its subsequent dispersion through and energy spread beyond the mask. There is also the potential risk of optically damaging the mask, if pulse energies or focusing conditions are not carefully constrained. With respect to the grating inscription schemes discussed so far, the femtosecond laser has been utilised as follows: Mihailov and co-workers [53–55] have developed phase masks designed for use at 800 nm for the inscription of quality, higher-order Bragg gratings in optical fibres. The use of phase masks with larger pitch mitigates pulse spreading, and gratings were produced having the dual advantage of good spectral quality and high thermal stability to 950°C. Martinez and co-workers [56, 57] have opted for point-by-point inscription of multiple-order gratings, with the third-order giving the best spectral quality. Computer-controlled systems are also under development for the formation of arbitrary and multiple Bragg gratings [58].

5.5 Fibre Bragg Gratings in Optical Communication Systems

The unique filtering properties of fibre Bragg gratings and their versatility as in-fibre devices have made FBGs one of the key components in fibre optic networks [1], and FBGs are used in ultra long haul (ULH), long haul (LH), and Metropolitan dense WDM (DWDM) telecommunication networks as well. A schematic representation of a network is depicted in Fig. 5.26. Bragg gratings are located in optical erbium-doped fibre amplifiers (EDFA) for pump wavelength stabilization and erbium-gain flattening as well as in add-drop nodes for wavelength filtering and multiplexing. They are also used in line or at the emission-reception side for channel and band dispersion compensation.

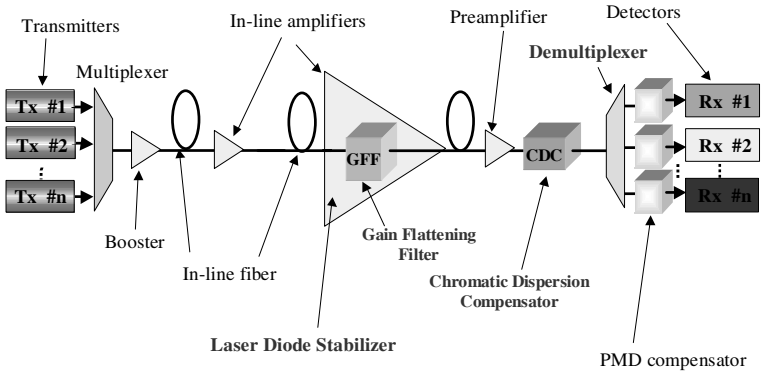

Fig. 5.26. Schematic representation of telecommunication network with preferred Bragg grating locations

Wavelength Channel Filters

Band-pass filters are key components of WDM systems, and many solutions utilizing fibre Bragg gratings for implementing such filters have been developed including Sagnac [59], Michelson [60, 61] or Mach–Zehnder [62, 63] interferometric configurations. Another approach, based on the principle of the Moiré grating resonator [64], has been applied with uniform period [65] and chirped [66] gratings. Resonant filter structures have been fabricated by introducing a phase shift into the grating by an additional UV exposure, or by using a phase-shifted phase mask. In general the resonant type transmission filters are capable of large wavelength selectivity and are, in principle, simple to manufacture and do not require carefully balanced arms or identical gratings, as in the case of interferometric filters.

Fibre Bragg 100-, 50- and 25-GHz bandwidth reflective filters are commercial products with low out-of-band crosstalk (better than 25 dB for the adjacent channel) and low chromatic dispersion (< 30 ps/nm for a 50 GHz grating). The realization of specific fibres (low cladding mode coupling fibre or high numerical aperture (HNA) fibre, cf. Sect. 5.2.5) is important in order to get these specifications with lowest possible losses (< 0.2 dB). One key application is channel selection in optical add-drop multiplexers.

Chromatic Dispersion Compensation

Chromatic dispersion is one of the key factors limiting transmission distances of 10 and 40 Gbit/s optical systems, and FBGs are widely used to mitigate these adverse effects. The phase response of a fibre Bragg grating can be designed to compensate many wavelengths and chirped fibre gratings are a well known (commercially available) solution for single channel and multi-channel dispersion compensation. The phase of the FBG is tailored during the photo-inscription process in order to get a linear variation of the delay as a function of wavelength. Dispersion compensation ranging from 100 to 2000 ps/nm has been demonstrated using chirped gratings. Many studies have focused on controlling the linear delay and suppression of the phase ripple inherent to multi-interference occuring inside the grating (< ±5 ps).

Tuneable dispersion gratings for 40 Gbit/s systems enable the compensation of slow dispersion variations in telecommunication networks (temperature and vibration effects), for example by the application of an external chirp to the grating by means of a mechanical strain or a temperature gradient. This external chirp can then be added to the one created during photo-inscription and leads to a dispersion tuning over a few hundred of ps/nm. Bragg gratings constitute the most efficient current technology for dispersion tuning. The main alternative technologies are planar devices and thin-film filters exploiting the Gires–Tournois effects (cf. Chaps. 6 and 7).

Gain-flattening Filters

In Metro, LH or ULH transmission systems optical amplifiers (EDFA) are necessary to compensate the link losses, and good overall amplifier flatness is required for low optical signal-to-noise ratio at all wavelengths. Different variants of Bragg gratings can be used to achieve this purpose. The FBGs can have non-uniform period (mostly linearly varying) to cover the full amplifier bandwidth, and these chirped gratings (cf. Sect. 5.3.2) are used in reflection with isolators on both sides. The major competitive

technology is dielectric thin film filters (cf. Chap. 7), which have inferior optical performance, but are available at lower cost, since they do not require optical isolators as FBGs do. To overcome this drawback slanted gratings have been developed [67]. They exhibit a tilt between the fibre axis and that of the grating in order to couple the forward-propagating fundamental mode (LP_{01}) to radiative modes which makes the filter dissipative in transmission. Different fibres have been designed to improve this coupling and suppress the residual backward wave (LP_{01-}). Total C-band transmission error functions lower than ±0.2 dB over the temperature range −10°C… +70°C have been demonstrated with induced losses smaller than 1 dB.

Pump Laser Stabilisation

Finally, fibre Bragg gratings are also used for the stabilisation of pump laser diodes in optical amplifiers. In EDFAs used in DWDM configurations, the precise stabilization of the pump wavelength is crucial. A small reflective grating is directly photo-written into the core of the laser pigtailed fibre. The feedback provided by the grating causes the laser to oscillate at the reflected wavelength, and most of today's pump laser diodes use a stabilizing grating written in standard or polarisation-maintaining fibre.

Gain flattening filters as well as Bragg grating-based add-drop multiplexers and dispersion compensators will be described in more detail in the following sections.

5.5.1 Add-drop Multiplexers

Fixed or reconfigurable optical add-drop multiplexers ((R)OADM) enable static or dynamic routing in wavelength division multiplexing networks, and AWGs (cf. Chap. 4), dielectric multilayer filters (cf. Chap. 7) or FBGs are most frequently used for the realisation of OADMs. The main advantages of FBG-based WDM filters are very high selectivity, flat top spectral response, steep spectral roll-off, and low insertion loss. As a consequence, FBG filters are widely used in low channel spacing (< 100 GHz) OADMs. The reflectivity and transmission spectra of a 50 GHz FBG are shown in Fig. 5.27. The grating is photo-written in a specific low-cladding-mode-loss fibre to avoid extra transmission losses out of the FBG spectral band. The complex apodization applied during the writing process assures an in-band dispersion lower than 10 ps/nm.

OADMs can be implemented in different configurations. One example is a passive temperature-compensated FBG sandwiched between two optical circulators (Fig. 5.28). If different wavelengths are injected at the input

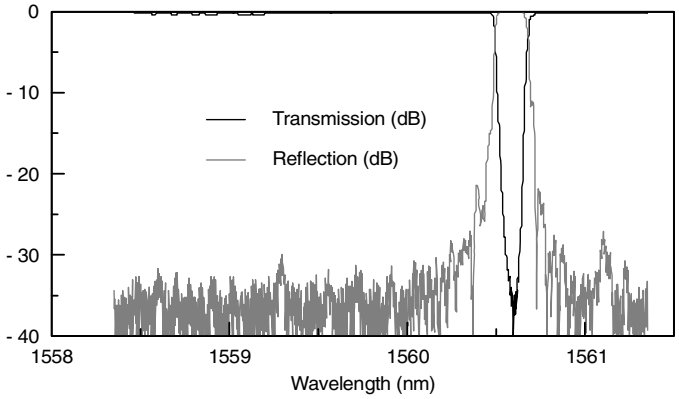

Fig. 5.27. Characteristics of 50 GHz fibre Bragg grating filter

port (1), the Bragg wavelength (λ_B) is reflected by the FBG and routed by the optical circulator to the drop port, while all other signals ($\lambda_i \neq \lambda_B$) pass through the FBG and exit via the output port (2). Since the component is symmetric, a new optical channel can be added (at λ_B) to the network through the add port, and the inserted wavelength exits the OADM from the output port (2) as well. Furthermore, if the FBG is made tuneable (thermally or by applying a mechanical force, cf. Sect. 5.2.4), its Bragg wavelength can change and the device becomes reconfigurable. Temperature-induced tuning over 8 nm with < 50 ms switching time has been demonstrated [68].

Placing Bragg gratings between optical circulators in a hybrid fashion is the simplest way of making FBG-based OADMs, but such devices exhibit high insertion loss and they are expensive. One option with no need of (expensive) circulators is a Mach–Zehnder interferometer (all-fibre solution) configuration with photo-imprinted Bragg gratings in each arm as illustrated schematically in Fig. 5.29. The device consists of two identical

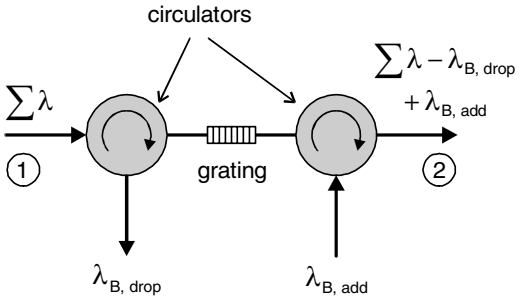

Fig. 5.28. Fibre Bragg grating-based add-drop multiplexer

FBGs and 3-dB couplers fused on both sides of the gratings, which makes the device a MZI for all wavelengths but the Bragg wavelength for which it is a Michelson interferometer. A signal launched into the input port is equally split through the first 3-dB coupler, and the Bragg wavelength is back-reflected on each arm of the MZI, while all other wavelengths pass through the FBG. Phase matching by UV trimming assures efficient extraction of the Bragg wavelength via the drop port. All other phase-matched wavelengths ($\lambda_i \neq \lambda_B$) leave the device via the output port, and a signal at the channel wavelength (λ_B) launched into the add port emerges at the output port as well (Fig. 5.29).

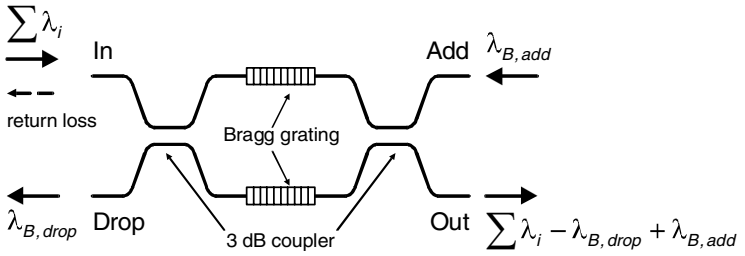

Fig. 5.29. Twin core fibre-based Mach–Zehnder interferometer add-drop multiplexer

The signal intensity propagating to the output and the add-port, respectively ($I_{in>out}$, $I_{in>add}$) as a function of the wavelength-dependent phase difference $\varphi(\lambda)$ between the arms, is given for the lossless case by (5.25) and (5.26), where $t_i(\lambda)$ is the complex transmission coefficient of the FBGs and $x_i(\lambda)$ the power coupling ratio of the couplers:

$$I_{in>out}(\lambda) = \left| \sqrt{(1-x_1)x_2} \cdot t_1(\lambda) \cdot \exp(\mathrm{i}\varphi(\lambda)) + \sqrt{(x_1(1-x_2))} \cdot t_2(\lambda) \right|^2 \cdot I_{in}(\lambda) \tag{5.25}$$

$$I_{in>add}(\lambda) = \left| \sqrt{(1-x_1)(1-x_2)}\, t_1(\lambda) \cdot \exp(\mathrm{i}\varphi(\lambda)) - \sqrt{x_1 x_2}\, t_2(\lambda) \right|^2 \cdot I_{in}(\lambda) \tag{5.26}$$

Similarly, $I_{in>drop}$ and the return loss $I_{in>in}$ can easily be obtained by (5.25) and (5.26), if all subscripts 2 are replaced by 1 and the reflection coefficients are used instead of the transmission coefficients.

Such MZIs can be realized using standard single-mode fibre or twin core fibre (TCF), where the TCF has a number of advantages compared to the SMF. Since the cores are embedded within the same cladding, the effective index difference between the arms is very small, and consequently

the chromatic dispersion of the MZI is essentially that of the couplers. TCFs allow a very reproducible fusion-tapering process as well, which means that the centre wavelength of the couplers can be well controlled. For example, for a 30 dB isolation between $I_{add>out}$ and $I_{add>add}$, the centre wavelength of couplers must be controlled within 5 nm.

The performance of a 200 GHz MZI OADM is illustrated in Fig. 5.30: The Bragg wavelength is extracted from the drop port with more than 30 dB adjacent crosstalk, the in-band rejection of the output port is better than 30 dB, and the crosstalk isolation between signals passing through the add and the output port is better than 30 dB over a 25 nm range. These results confirm that the couplers exhibit very low chromatic dispersion and are well centred at the Bragg wavelength. The return loss reaches 18 dB in-band, while it is better than 25 dB over 30 nm out-of-band. It is worthwhile to note that the measurements have been performed on SMFs coupled to the TCFs, and total insertion loss of any path is better than 1.5 dB. Bit error rate measurements at 10 Gbit/s using this device did not show any power penalty at all [69].

Passive athermal add-drop devices have been demonstrated with less than 1 pm/°C deviation of the Bragg wavelength over the −10°C to +70°C temperature range [70–72]. Theoretical analyses of MZI-OADMs have demonstrated that the phase mismatch of the Bragg gratings (leading to Bragg wavelength detuning) is the most critical parameter determining in-band return loss.

Recent studies focused on the realization of MZI-based add-drop multiplexers in planar waveguide architecture with large negative index

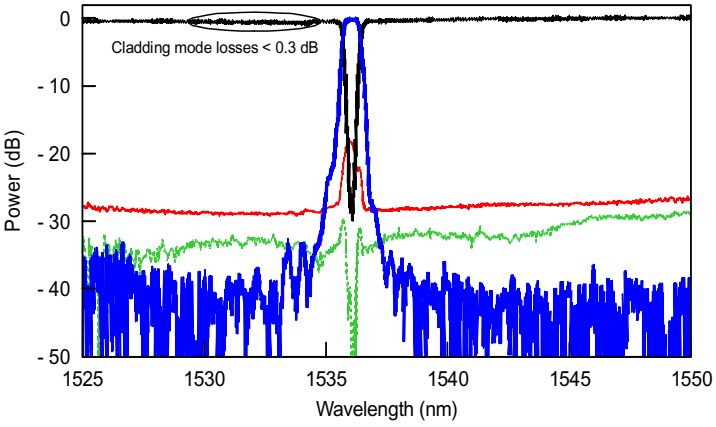

Fig. 5.30. Optical performance of packaged 200 GHz twin core fibre-based OADM. Transmission: black; drop (reflection): blue; return loss: red; input to add channel: green

modulation. Moreover, efficient thermal tuning of a Mach–Zehnder-based OADM has been demonstrated over 1.7 nm without significant modification of the drop directivity and the throughput signals.

Table 5.1 illustrates the performance of FBG-based hybrid and all-fibre fixed 100 GHz optical add-drop multiplexers.

Table 5.1. Characteristics of FBG-based hybrid and in-fibre, fixed 100 GHz OADMs

Optical parameter	Hybrid OADM	In-fibre OADM
Insertion loss (dB)	1.5	1.5
Isolation (dB)	30	30
Rejection (dB)	30	30
In-band return loss (dB)	30	20
Out-of-band return loss (dB)	30	30

Sub-band and single wavelength Bragg grating-based OADMs in fibre or/and planar waveguide technology are still topics of current research, and in particular SiO_2/Si offers the potential for the realization of complex multi-wavelength functionalities.

A device rather similar to the add-drop multiplexer is a single Bragg grating in a single-mode fibre acting as a wavelength selective distributed reflector or a band-rejection filter by reflecting wavelengths around the Bragg resonance. By placing identical gratings in two lengths of a fibre coupler, as in a Michelson arrangement, one can make a band-pass filter [73]. This filter, shown in Fig. 5.31, passes only wavelengths in a band around the Bragg resonance and discards other wavelengths without reflections. If the input port is excited by broadband light and the wavelengths reflected by the gratings arrive at the coupler with identical optical delays, then this wavelength simply returns to the input port. If, however, a path-length difference of $\pi/2$ is introduced between the two arms, then it is possible to steer the reflected wavelength to arrive at the second input port, creating a bandpass filter. In principle, this is a low-loss filter, although there is a 3 dB loss penalty for the wavelengths that are not reflected, unless a Mach–Zehnder interferometer is used to recombine the signal at the output [60]. An efficient band-pass filter was demonstrated by Bilodeau et al. [61] using a scheme identical to that presented in reference [60]. The device had back reflection of −30 dB (cf. Glossary for definition). However, all wavelengths out of the pass-band suffered from the 3-dB loss associated with the Michelson interferometer.

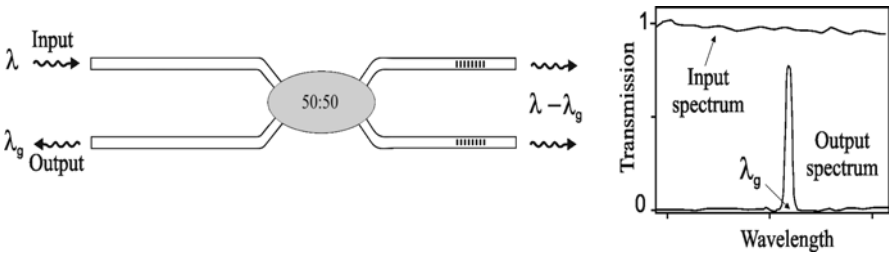

Fig. 5.31. Fibre-optic bandpass filter using Bragg reflectors arranged in a Michelson-type configuration

5.5.2 FBG-based Chromatic Dispersion Compensators

The group velocity of optical signals travelling along a fibre is wavelength-dependent due to material and waveguide dispersion, and this phenomenon is usually called chromatic dispersion (CD). Waveguide dispersion is essentially due to a wavelength-dependent distribution of light between the core and the cladding of a single-mode fibre. Due to CD pulses propagating along an optical fibre experience a temporal broadening which limits the maximum transmission distance since subsequent pulses become overlapping, i. e. one gets inter-symbol interference. Tolerable chromatic dispersion depends on the modulation format, the channel wavelength, the spectral width of the pulses, the fibre type, and on the bit rate. To a first approximation tolerable chromatic dispersion decreases proportional to the square of the bit rate, so its effect becomes significant for 10 Gbit/s and beyond, and different techniques have been developed in the past to compensate unwanted chromatic dispersion, so that the maximum optical span length is extended. An estimate of dispersion-limited maximum transmission lengths (1 dB power penalty) for standard transmission formats and without dispersion compensation is given by [74]

$$B^2 DL \leq 10^5 \tag{5.27}$$

where B is the bit rate, L the fibre length, and $D(\lambda)$ the fibre chromatic dispersion. For a Corning SMF-28e fibre, for example, $D(\lambda)$ (in [ps/(nm·km)]) is given by

$$D(\lambda) \approx \frac{S_0}{4}\left[\lambda - \frac{\lambda_0^4}{\lambda^3}\right] \tag{5.28}$$

for the wavelength range $1200\,\text{nm} \leq \lambda \leq 1625\,\text{nm}$, where λ_0 is the zero dispersion wavelength ($1302\,\text{nm} \leq \lambda_0 \leq 1322\,\text{nm}$) and S_0 is the zero dispersion

slope: $S_0 \leq 0.092\,\mathrm{ps}/(\mathrm{nm}^2 \cdot \mathrm{km})$ [75]. Table 5.2 illustrates that dispersion poses severe limits on the maximum transmission distances at higher bit rates and consequently dispersion compensation is of high relevance at higher bit rates.

Table 5.2. Dispersion-limited maximum transmission distance for standard single-mode (SMF-28) and non-zero dispersion shifted fibre (1 dB penalty, no dispersion compensation)

Bit rate	Transmission over SMF-28	Transmission over NZ-DSF
2.5 Gbit/s	1000 km	6000 km
10 Gbit/s	60 km	400 km
40 Gbit/s	4 km	25 km

One well established, broadband solution for compensating CD is the use of dispersion-compensating fibre (DCF). A DCF has a high negative dispersion (at 1.5 µm) which is several times larger than the positive dispersion of a standard SMF. However, DCF exhibits rather high losses (typically 10 dB for 80 km fibre), high non-linearity due to a small mode effective area, and the use of DCF adds extra cost because extra amplifiers are needed to compensate the DCF loss. Moreover, for certain system configurations only single wavelengths or sub-band dispersion compensation is needed (4, 8, or 16 wavelengths), and DCF is not particularly suited to accomplish this task. Finally, in particular at 40 Gbit/s, tuneable dispersion compensation is requested in order to precisely compensate the dispersion for each channel and to correct for environmentally-induced variations, and DCF cannot meet these requirements.

On the other hand, chirped fibre Bragg gratings enable versatile and efficient dispersion compensation. The first practical demonstrations of dispersion compensation by means of chirped FBGs used short pulses of either 1.8 ps [76] or 21 ps [77] duration.

The design of a dispersion-compensating module (DCM) consisting of a 3-port circulator and a chirped grating and operating in reflection is illustrated schematically in Fig. 5.32.

The index modulation of the grating is given by

$$n(z) = n_{eff} + \Delta n_{\mathrm{mod}} \times f_{apod}(z) \times \cos\left(\frac{2\pi}{\Lambda} z - \frac{\pi}{2\, n_{eff} \Lambda^2} \Lambda_1 z^2\right) \qquad (5.29)$$

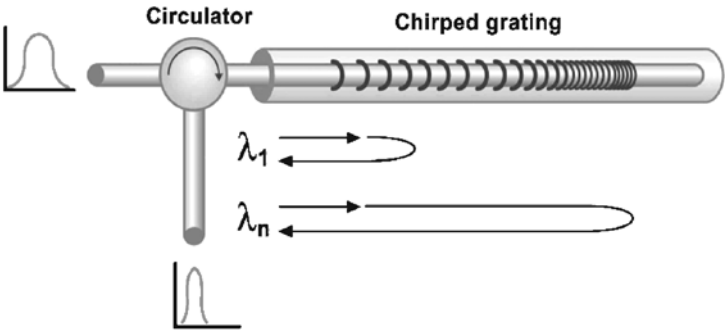

Fig. 5.32. Dispersion compensating module (schematic, $\lambda_1 > \lambda_n$)

where n_{eff} is the mean effective index, $n(z)$ is the index variation along the fibre axis, Λ is the grating mean pitch, Δn_{mod} is the index modulation amplitude, $f_{apod}(z)$ is the apodization function, and Λ_1 is the so-called chirp parameter of the Bragg wavelength (see (5.22)) which ensures a linear variation of the local Bragg wavelength along the grating via the variation of the pitch or/and of the effective index. The spectral bandwidth of the grating increases with the grating length, and different wavelengths are reflected at different spatial locations inside the grating. Shorter wavelengths are reflected towards the end of the grating and are thus delayed with respect to longer wavelengths which are reflected at the beginning of the grating.

The delay τ, the bandwidth $\Delta\lambda$, and the dispersion D associated with the chirped grating are linked by the following set of equations :

$$\tau = \frac{2n_g L_g}{c} \tag{5.30a}$$

$$\Delta\lambda = \Lambda_1 \times L_g \tag{5.30b}$$

so that

$$D = \frac{\tau}{\Delta\lambda} = \frac{2n_g}{c \times \Lambda_1} \tag{5.31}$$

where n_g is the fiber group index, L_g the grating length, and Λ_1 the chirp parameter.

Chirped gratings can be realized in different ways. The most popular approach uses a chirped phase mask and a standard photo-inscription set-up. An alternative is to use a standard uniform phase mask and then apply a specific back and forth movement of the fibre in front of the phase mask [78]. A further option is to taper the fibre continuously (by fusion) in order

to generate a continuous change of the refractive index along the fibre in the region where the grating is to be inscribed [79]. A uniform phase mask is then used to photo-write the grating.

Figure 5.33 shows the reflectivity and the resulting group delay of a linearly chirped FGB-based DCM. This component has been written according to the second method using an excimer laser (10 mJ, 200 Hz) and a standard uniform phase mask ($\Lambda = 1066.0$ nm). Moving the fibre in front of the mask introduced a chirp of 0.185 nm/cm, and according to (5.31) the resulting dispersion is equal to –530 ps/nm. The grating length was 70 mm and the apodization function an hyperbolic tangent.

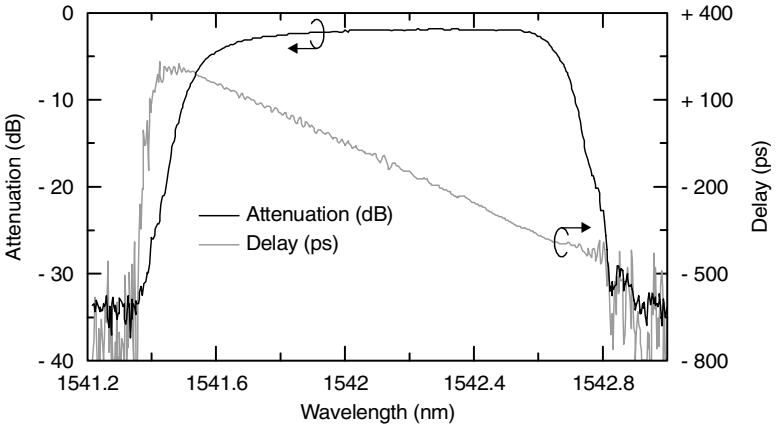

Fig. 5.33. Reflectivity and group delay spectrum of a chirped FBG-based DCM

Figure 5.33 shows a linear variation of the group delay over the filter bandwidth (constant dispersion), and the existence of a residual ripple on the delay curve can also be seen which will be explained below. In principle, the dispersion can be positive or negative, depending on the propagation direction of the beam in the grating region. Dispersion ranging from –2000 ps/nm to +2000 ps/nm has been demonstrated with module insertion loss < 2 dB.

FBG-based dispersion compensators are not restricted to operate over narrow wavelength bands only. As the delay increases with the grating length, one possibility to achieve broadband operation is making long FBGs (length > 1 meter). However, such devices are very difficult to realize and the group delay ripple is generally too high for network applications.

Another option is phase- or amplitude-sampled gratings [80]. Such components require a large number of phase shifts along the grating length. The expression of the index modulation $\Delta n_{mod}(z)$ in sampled gratings is given by

$$\Delta n_{\mathrm{mod}}(z) = \Delta n_0 \; f_{\mathrm{apod}}(z) \sum_{m=1}^{M} \cos\left(\frac{4\pi \, n_{\mathrm{eff}} \, z}{\lambda_0 + \Delta\lambda_{\mathrm{m}}} + \phi_{\mathrm{m}} \right)$$
$$= \Delta n_0 \; f_{\mathrm{apod}}(z) \; A_{\mathrm{sampl}}(z) \cos\left(\frac{4\pi \, n_{\mathrm{eff}} \, z}{\lambda_0} + \phi_{\mathrm{sampl}}(z) \right) \tag{5.32}$$

where Δn_0 is the index modulation amplitude for a single channel, M is the number of channels, $\Delta\lambda_m$ is the spectral spacing between the m^{th} channel and the central wavelength λ_0, and ϕ_m is the phase of the m^{th} channel.

In the case of amplitude sampling (i. e. the case when $\phi_{sampl}(z) = \mathrm{const}$) there are dead zones, where no gratings are photo-written, and these lower the reflectivity of the FBG as the number of WDM channels increases.

The phase-sampling method (i. e. the case when $A_{sampl}(z) = \mathrm{const}$) is an alternative that overcomes these difficulties [81]. Since the refractive index modulation Δn required to maintain the reflectivity is much lower than that for the amplitude-sampling method, phase-sampled gratings can be fabricated more easily. Without using specially designed phase masks, phase-sampled FBGs have been realized by dithering and displacing standard phase masks. Phase-sampled gratings represent the most promising approach to realize multichannel DCM, but a very precise photo-inscription set-up and processing are mandatory [82].

A further variant of multi-channel DCM relies on the superposition of multiple Bragg gratings implemented over an arbitrary large range of wavelengths [83]. This third alternative, called superimposition, involves inefficient fabrication processes, because several FBGs are overwritten in the same location of a fibre, and each FBG corresponds to one channel. On the other hand, an advantage of the superimposed approach is that the separate FBGs are independent from each other. This allows the design of complex structures including channel to channel varying dispersion, which is useful for dispersion-slope compensation.

Multichannel FBG-based DCM offer many advantages compared to DCF, e. g. small footprint, low insertion loss, dispersion-slope compensation, and negligible non-linear effects. Table 5.3 compiles characteristic parameters of single- and 32-channel dispersion-compensating modules.

Table 5.3. Characteristics of single- and 32-channel chirped FBG-based dispersion-compensating modules

Parameter	Single-λ DCM	32-λ DCM
Channel bandwidth (GHz)	20 to 80	30
Insertion loss (dB)	1.5 (with circulator)	< 3.5
Dispersion (ps/nm)	−2000 to +2000	−2000 to +2000
Group delay ripple (ps)	< ±10	< ±40
PMD (ps)	< 0.5	< 0.5
PDL (dB)	< 0.1	< 0.3
Athermal package size	168 mm length, 12 mm diameter	209 mm length, 14 mm diameter
Operating temperature (°C)	−5 to +70	−5 to +70

5.5.3 Tuneable Dispersion-compensating Module

Dynamic dispersion compensation is essential in DWDM optical communication systems operating at 40 Gbit/s and beyond. At these high bit rates, dispersion tolerances become so small that variations in dispersion can severely influence network performance. In such systems the amount of dispersion compensation required at the receiver to maintain optimum system performance may vary in time due to impairments which exhibit temporal variations. Factors which contribute to total dispersion are temperature fluctuations along the fibre, component dispersion, and dispersion variations in the transmission fibre. For example, for a 2000 km non-zero dispersion shifted fibre (NZDSF) span, a 10 to 20°C temperature change is sufficient to introduce measurable system impairments at 40 Gbit/s. Furthermore, in reconfigurable networks the total accumulated dispersion can experience significant sudden changes.

Chirped FBGs combined with an appropriate tuning platform are well suited for single or multiple channel dispersion compensation. Tuning can be achieved by creating a temperature gradient along the fibre [84] or by applying a linear strain gradient which can be provided by the S-bending beam technique for example [85]. Most commercially available tuneable dispersion-compensating modules (TDCM) use two (or more) thermoelectric coolers (TEC) located at each end of the grating. A thermal gradient is then created along the fibre, while the temperature at the centre is kept unchanged. This controllable temperature gradient generates chirp and thus dispersion variation. The chirp can be adjusted reversibly by varying the TEC current. If the grating in a DCM has an intrinsic chirp, the total chirp is the algebraic sum of both chirp contributions (intrinsic and reversible, TEC-induced one). As the total chirp is increased, the component

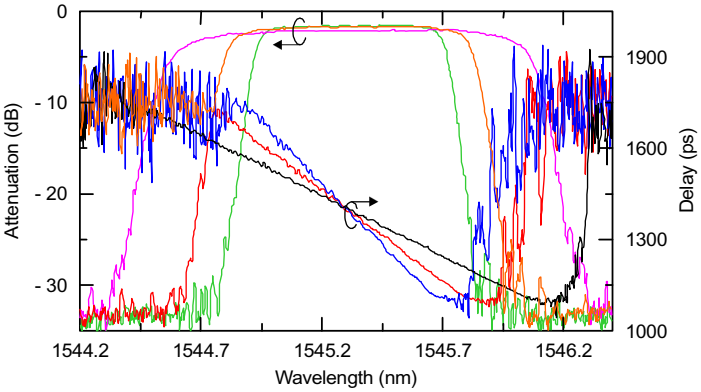

Fig. 5.34. Evolution of the spectral response of a dispersion-compensating module with tuning

bandwidth is increased, so that the delay slope, i. e. the dispersion, is reduced (in absolute terms). Corresponding integrated devices satisfy important requirements such as power efficiency, small size, and ease of fabrication. Figure 5.34 shows the evolution of the spectral bandwidth and the delay of a tuneable DCM.

It is important to note that with this architecture the Bragg wavelength is fixed, and that tuneability around a zero dispersion value is not possible. These spectra also show that the maximum reflectivity is not the same as the temperature gradient is changed. For the case of thermal tuning Fig. 5.35a illustrates the resulting non-linear dispersion variation for a grating with an initial dispersion value of –533 ps/nm.

As the index modulation is constant, the dispersion tuning is associated with a variation of the grating reflectivity. In the example of Fig. 5.35a it corresponds to 0.5 dB insertion loss variation.

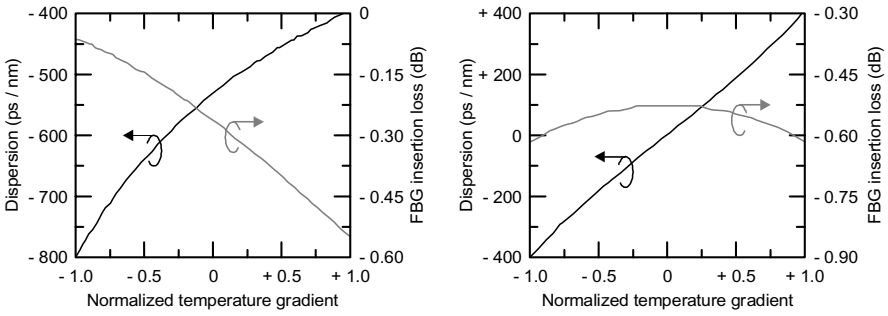

Fig. 5.35. Tuning characteristics examples of (**a**) single grating and (**b**) twin gratings configuration (after [86])

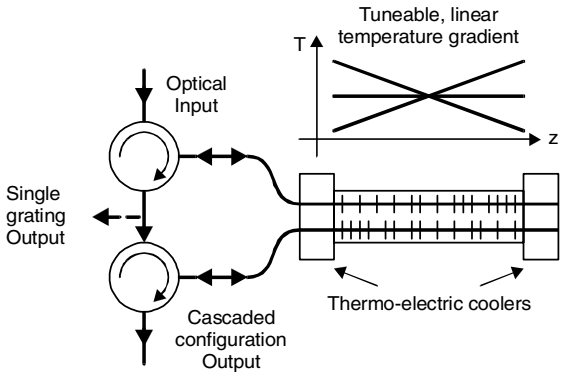

Fig. 5.36. Temperature tuning principle scheme (after [86])

Another configuration also using thermal tuning is illustrated in Fig. 5.36. Key elements are two identical, chirped cascaded FBGs and two 3-port circulators. Both gratings are simultaneously tuned (similar to the case of a single FBG), but the key point is that the chirp of the two FBGs varies in opposite directions with respect to the temperature gradient. As the sign of the dispersion of a chirped FBG changes with propagation direction, the total dispersion is zero without applied temperature gradient [86]. A temperature gradient induces opposite bandwidth variations for each grating. The tuning characteristics can simply be deduced from the single grating case (one has to keep in mind that transmission losses are expressed in decibels and dispersion values simply add). The tuning range (Fig. 5.35b) is now centred around zero and is doubled without any additional power consumption. The insertion loss variation with tuning is considerably reduced (less than 0.1 dB in this example) because both reflectivity variations cancel each other. Another interesting point is the quasi-linear relation between the applied gradient and the resulting dispersion, i. e. one gets a quasi-constant tuning sensitivity.

With a maximum temperature variation of 60°C the dispersion tuning range extends from −400 to +400 ps/nm. The total electrical power consumption of this component is 5 watts during the transient regime and 3 watts in the stationary state.

Mechanical designs are also very attractive [87], but they are only suited for applications with no need to permanently adjust the dispersion. The advantage of such a ‘set and forget’-device is that there is no electrical power consumption except when it is tuned to the proper dispersion compensating value.

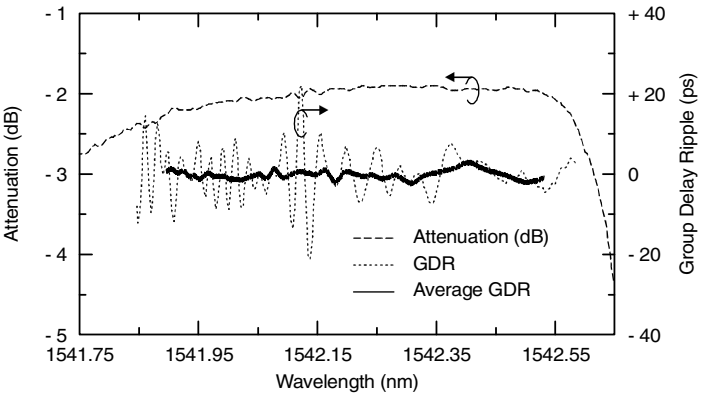

Fig. 5.37. Reflectivity (*dashed*), group delay ripple after subtracting a polynomial fit of the delay over the 0.5 dB bandwidth (*dotted*), and mean group delay ripple with a 100 pm resolution (*heavy line*)

5.5.4 Ripple Analysis in Dispersion-compensating Modules

The main limitation of chirped fibre Bragg grating (CFBG) technology is currently given by the well-known phase ripple (cf. also Chap. 2, Sect. 2.4.3) which is due to a non-optimum apodization function and/or imperfections related to the photo-inscription process. Although ripples can be equivalently characterized by the dispersion, the group delay, or the phase spectrum, respectively, there was until recently an implicit preference for directly measured group delay spectra (Fig. 5.37). However, very recent work showed that characterising the ripple over the phase spectrum instead of the group delay spectrum provides significant advantages. In addition, there is clear evidence that minimizing the group delay ripple (GDR) amplitude is not enough to reduce the impact on system performance, but the GDR period is also of high importance [88].

The worst case eye-opening penalty (EOP) associated with the use of a DCM can be calculated from the period and the amplitude of the group delay ripples [89] which can be separated into high and low frequency ones (Fig. 5.37). The latter are associated with a slowly varying curve, which gives a residual dispersion and leads to a broadening of the input pulse. The corresponding system impact can be estimated with conventional techniques. High frequency ripples are much more complicated to understand and to correct as well. They create new pulses which interfere with adjacent pulses. For a given GDR amplitude highest system impairments occur when the GDR period, expressed in optical frequency units,

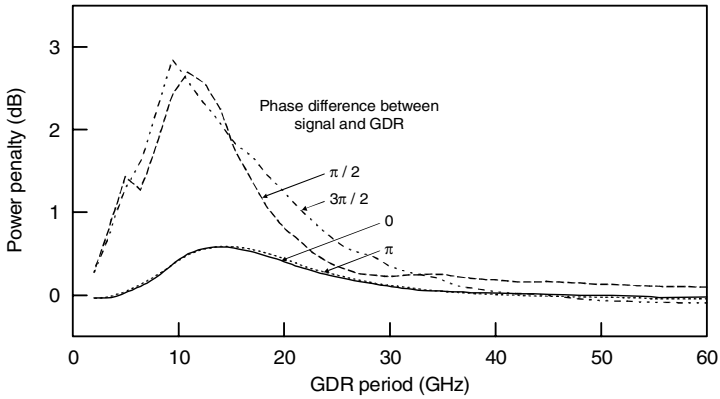

Fig. 5.38. Penalty versus group delay ripple (GDR) period for different phase differences between signal and ripple (NRZ modulation format, 10 Gbit/s)

equals the bit rate (10, 40 Gbit/s). For a high frequency sinusoidal ripple the EOP is approximately proportional to the product of the GDR amplitude and period [90], (cf. Fig. 5.38), i. e. to the phase-ripple amplitude.

One approach to determine the impact of GDR ripple on a telecommunication system is known as wavelength-frequency signal analysis based on spectrogram distributions (a method more commonly used in mechanical vibration analysis). The method reveals the variation of the frequency spectrum with respect to wavelength, and it provides useful information on the presence or absence of specific periods (ripple with 80 pm or 320 pm period is particularly detrimental for 10 or 40 Gbit/s systems, respectively) and on their localization inside the component bandwidth. It also helps to differentiate between apodization-induced and index variation noise-induced GDR [91], and it enables linking the measured penalty spectrum with the spectrogram and to correlate the peak penalty and critical frequencies in the GDR at the same wavelength as well.

An alternative approach to determine the impact of GDR on system performance is based on phase measurements since the phase ripple magnitude is a good indicator of system performance as long as it includes high frequency ripple components only. This is outlined in more detail in recent publications [92–94].

5.5.5 Gain-flattening Filters

Gain-equalized optical amplifiers have allowed the deployment of new DWDM systems. Power uniformity over the communication bandwidth is an important requirement in such systems since flatter optical amplifier

gain enables longer fibre spans between regenerators which is more cost effective. Moreover, gain flatness of EDFAs is necessary to improve the optical signal-noise ratio. The straightforward option for gain equalization is the insertion of a gain flattening filter (GFF) with a spectral response precisely tailored to the inverse gain profile. In addition to exhibiting a spectral shape as close as possible to the inverse EDFA gain curve, GFFs should have low polarisation dependence, small footprint, and low loss.

Several technologies have been developed to perform gain equalization. The most common choice is dielectric thin film filters (cf. Chap. 7) which are particularly attractive with respect to cost due to high volume production. Long period gratings (LPG) [95] would in principle be a second possibility, however, they did not find any significant use with EDFAs due to their poor ageing characteristics (in particular, UV LPG). Finally, chirped and slanted/chirped short period FBGs form the last technology option, and best specifications have been obtained so far with this approach. Their superior performance combined with their good ageing behaviour and package reliability have led the main sub-marine carriers to use this technology.

Characteristic data of GFFs realized using different technologies are listed in Table 5.4.

Table 5.4. Comparison of gain-flattening filters based on different technologies (after [96])

Characteristics over full T range	**Thin-film Filter**	**Long-period Grating**	**Grade A Chirped GFF**	**Slanted/ Chirped GFF**
Error function	± 0.5 dB	± 0.5 dB	± 0.1 dB	± 0.2 dB
PDL	< 0.1 dB	< 0.2 dB	< 0.1 dB	< 0.1 dB
PMD	n.a.	n.a.	< 0.1 ps	< 0.1 ps
Insertion loss (out of band)	1 dB	0.3 dB	0.3 dB	0.5 dB
Back reflection	low	low	high	low
Temperature dependence	< 5 pm / °C	< 3 pm / °C	< 1 pm / °C	< 1 pm / °C
Dimensions	small	large	small	small

The fabrication of short period chirped FBGs for GFFs starts by using a chirped phase mask to change the period of the fringe pattern along the length of the grating and by adjusting the induced index modulation to match the required transmission. This adjustment can be made by blurring the fringes with a displacement of the phase mask in front of the fibre during the photo-inscription process. These filters are compatible with

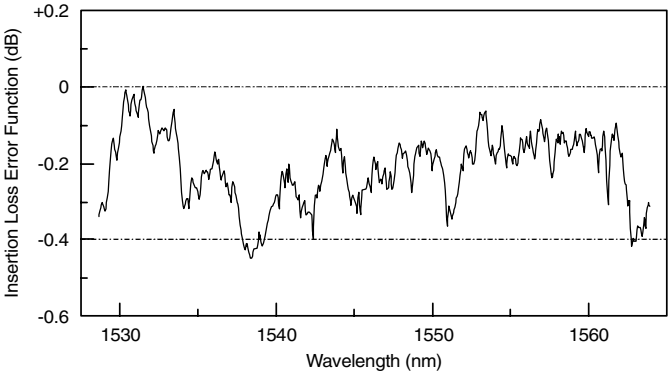

Fig. 5.39. Residual insertion loss variation of a gain-compensated EDFA

standard SMF-28 fibre and in most cases no particular fibre is needed, although fibres with a specific refractive index and photosensitivity profile may more efficiently suppress perturbations due to cladding mode coupling. The short piece of (specific) fibre with the grating is then spliced and sandwiched between two standard fibres. The GFF component itself is incorporated into the EDFA mostly in the middle of the erbium-doped fibre in order to avoid noise degradation. Losses are generally low and adequate annealing and packaging (hermetic sealing or fibre metallization) assure long term stability (> 25 years).

The main drawback of these filters, which are reflective filters used in transmission, is the need of optical isolators in order to avoid feedback inside the amplifier stage, which results in additional losses and higher overall cost. Furthermore, even if the induced dispersion and group delay ripple in transmission are very small (< ±2 ps around zero dispersion), the CFBG can sometimes lead to multi-path interference phenomena and pulse echoes shifted in time by a quantity equal to the reciprocal of the ripple modulation period. However, experiments show that group delay ripple of gain-flattening filters based on chirped FBGs do not cause significant system impairment at 10 and 40 Gbit/s [97]. Residual gain variations can be reduced to ±0.2 dB as illustrated in Fig. 5.39, and one of the key parameters to get ultra low flatness over the whole gain curve is the quality of the phase mask.

An alternative to standard GFFs are slanted chirped short period gratings (SCG) which offer a number of advantages compared to standard CFBG gain-flattening filters. Instead of coupling the power into the counter-propagating mode (reflective filter), slanted gratings direct the energy into the radiative modes (cf. Sect. 5.3.4). In order to minimize the residual coupling into the counter-propagating mode, a specific index profile-fibre is

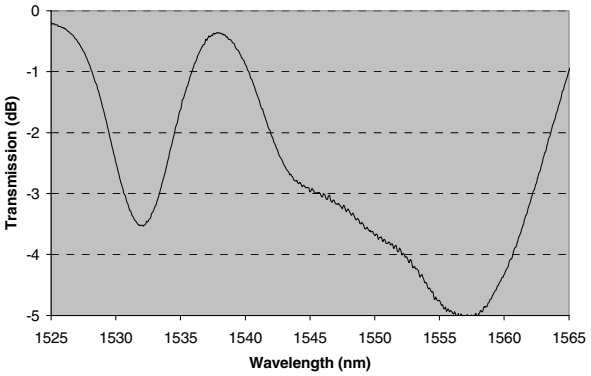

Fig. 5.40. Spectral shape of gain-flattening filter based on a slanted chirped grating

used with an adequate photosensitive profile. These two profiles are different, and different photosensitive species (like germanium or boron) can be used to obtain the required photosensitivity. Similar to standard chirped gratings, these slanted gratings are also chirped, i. e. the period of the fringe pattern changes along the grating (typical chirp is 10 nm/cm). The induced index modification is longitudinally adjusted to match the required transmission, and the spectral shape of the filter characteristics is the convolution of this blurred profile with the slanted grating elementary response. The final result is a smooth large band filter with a global shape very close to the complementary EDFA shape (Fig. 5.40). Using this component flatness smaller than 0.1 dB peak to peak has been demonstrated. The residual flatness is determined by the grating angle θ (larger cell for higher angle), the fringe pattern visibility, and the UV spot size.

The high frequency ripple which is relatively important in standard chirped GFFs (±0.1 dB) is reduced to less than ±0.02 dB for SCGs. Such low ripple is obtained by recoating the component with a polymer with an index greater than that of silica which suppresses cladding modes associated with high frequency ripple. The size and packaging of SCGs are similar to those of standard chirped gratings. Athermal Telcordia-qualified products for terrestrial and sub-marine applications are commercially available.

The residual reflectivity of slanted chirped FGBs can be made smaller than −25 dB, thus the requirements on optical isolation are relaxed compared to standard gratings, and in some EDFA configurations one single-stage isolator is sufficient instead of two two-stage isolators.

In telecommunication systems it is not only the gain flatness of a single EDFA which matters, but also the behaviour of cascaded EDFAs. If the GFF technology used exhibits systematic errors (such as dielectric multilayer filters, for example), the total error accumulates linearly with

the number of amplifiers, and the resulting error at the end of a chain of EDFAs has to be corrected by a clean-up filter or by signal regeneration. Chirped (slanted) GFFs exhibit a small systematic error and a high degree of random error (manifesting itself primarily by the high frequency ripple), and cascading these components causes a statistical error accumulation which is less serious than linear accumulation. For example, a peak-to-peak flatness per GFF better than 0.1 dB for a chain of 10 cascaded EDFAs has been demonstrated [98].

The polarisation-dependent loss of chirped or SCGs is small (< 0.1 dB), but it can sometimes be detrimental for a system. The PDL spectral shape can be explained by considering that it comes from a birefringence-induced spectral splitting of the two polarisation axes [99]. This effective index birefringence can be explained by an asymmetric UV-induced refractive-index profile across the fibre core due to the absorption of the writing UV-laser beam. This residual PDL can be reduced by double-side exposure of the fibre.

5.5.6 Wavelength Tuning and Chirping of Bragg Gratings Using Infrared Lasers

Kalli and co-workers reported the first experimental measurements on the spectral modification of fibre Bragg gratings (Type IA), resulting from high-power, near infrared laser irradiation [100]. The grating properties were modified in a controlled manner by exploiting the characteristics of the inherent 1400 nm absorption band of the optical fibre, which grows during the grating inscription and is due to the optical fibre pre-conditioning. Therefore, the increase in absorption occurs in the grating region. Illuminating the area with a high power laser having an emission wavelength coincident with the absorption band, produced reversibly modified centre wavelength and chirp. Furthermore, partial and permanent grating erasure was demonstrated.

A low power (10 mW) laser source coinciding with the absorption peak at 1400 nm induced small but significant wavelength shifts of approximately 100 pm. This wavelength shift would change the grating's spectral response adversely affecting the filter performance and reducing the isolation between wavelength channels, transmission properties, and effective bandwidth. A second source operating at 1425 nm and far from the absorption peak induced wavelength shifts in excess of 750 pm and a 30% increase in FWHM for a pump power of 350 mW. This has serious implications on all grating types when the fibre undergoes photosensitivity pre-conditioning, as their spectrum can be modified using purely optical methods (no external

heat source acts on the fibre), and it is also of relevance for long-term grating stability. It should be noted that high power lasers are increasingly being used in optical networks and this study may have greater implications to all grating types, as laser powers and the useable wavelength spectrum increase. This may result from the presence of absorption features in the visible and near infrared that are produced due to the fibre being preconditioned, prior to grating inscription (as in this case). Absorption features are observable at shorter wavelengths for conventional Type I gratings inscribed in hydrogenated fibre. Although there is no evidence that they have consequences for grating lifetime, their impact (or negligible impact) has still to be established conclusively.

Conversely, there are applications where suitably stabilized Type IA gratings can be spectrally tailored for tuning fibre lasers or modifying edge filters in sensing applications. The latter results from the non-uniform absorption of the pump laser source as it traverses the Type IA grating. The fact that this type of spectral tuning can be realized by the use of an additional laser source can be advantageous, as no special coatings to the fibre are necessary, and all degrees of tuning can be set during the grating manufacturing process which offers great flexibility at the design stage. Since all grating types can be written in a section of pre-exposed fibre, this method of optical tuning could be used for all existing Bragg grating applications making the technique invaluable to a multitude of applications. Finally we note that it is possible to tailor the absorption of the pre-exposed section to mirror the decay in intensity resulting in a uniform heating of the grating. However, this would alter the mean fibre index along the pre-exposed section, inducing a potentially large (up to 20 nm) chirp across the grating.

5.6 Other Applications of Fibre-based Bragg Gratings

Beyond their use in telecommunication systems fibre Bragg gratings have emerged as important components in a variety of other lightwave applications such as wavelength stabilized lasers, fibre lasers, remotely pumped amplifiers, Raman amplifiers, phase conjugators, or wavelength converters for example, and they are also considered excellent sensor elements, suitable for measuring static and dynamic fields such as temperature, strain, and pressure [101]. The principal advantage is that the information to be determined is wavelength-encoded (an absolute quantity) thereby making the sensor self-referencing, rendering it independent of fluctuating light levels and the system immune to source power and connector losses that plague

many other types of optical fibre sensors. It follows that any system incorporating Bragg gratings as sensor elements is potentially interrupt-immune. Their very low insertion loss and narrowband wavelength reflection offers convenient serial multiplexing along a single monomode optical fibre. There are further advantages of the Bragg grating over conventional electrical strain gauges, such as linearity in response over many orders of magnitude, immunity to electromagnetic interference (EMI), light weight, flexibility, stability, high temperature tolerance, and even durability against high radiation environments (darkening of fibres). Moreover, Bragg gratings can easily be embedded into materials to provide local damage detection as well as internal strain field mapping with high localization, strain resolution, and measurement range. The Bragg grating is an important component for the development of smart structure technology, with applications also emerging in process control and aerospace industries. This section will describe in brief some applications of fibre gratings.

5.6.1 Fibre Bragg Grating Diode Lasers

A fibre Bragg grating may be coupled to a semiconductor laser chip to obtain a fibre Bragg diode laser [102]. A semiconductor laser chip is antireflection coated on the output facet and coupled to a fibre with a Bragg grating as illustrated in Fig. 5.41. If this Bragg grating reflects at the gain bandwidth of the semiconductor material it is possible to obtain lasing at

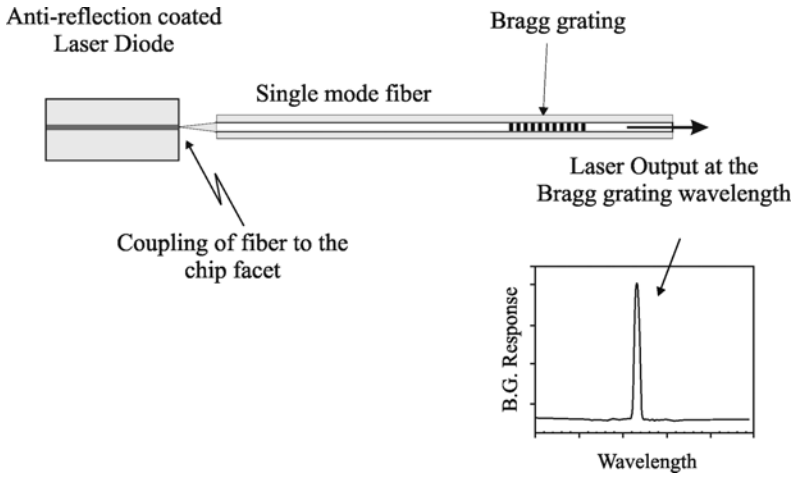

Fig. 5.41. External cavity fibre grating semiconductor laser. Semiconductor laser chip is antireflection coated on the output facet and coupled to a fibre with a Bragg grating, forcing oscillation at the Bragg grating wavelength

the Bragg grating wavelength. The grating bandwidth can be narrow enough to force single frequency operation with a linewidth of much less than a GHz. High output powers up to tens of mW have been obtained with these types of lasers. An added advantage of these systems is their temperature sensitivity, which is approximately 10% of that of a semiconductor laser, thus reducing temperature induced wavelength drift. These fibre grating semiconductor laser sources have been used to generate ultrashort mode-locked soliton pulses up to 2.9 GHz [103].

A manufacture problem in DBR lasers is the precise control of the laser wavelength. Routine production of DBR lasers with wavelength specified to better than 1 nm is difficult. On the other hand, Bragg gratings can be manufactured precisely (better than 0.1 nm) to the wavelength required. With anti-reflection coating on the semiconductor chip, the lasing wavelength may be selected from anywhere in the gain bandwidth by choosing the appropriate fibre Bragg grating. Clearly, such an approach will increase the yield from semiconductor wafers. In addition, since each laser has to be coupled to a fibre, the Bragg grating may be written after the packaging process has proved to be successful, thus reducing the time spent on unsuccessful products.

5.6.2 Fibre Bragg Grating Lasers

The majority of Bragg grating fibre laser research has been on erbium-doped lasers due to their potential in communication and sensor applications. The characteristic broadband gain profile of the erbium-doped fibre around the 1550 nm region makes it an extremely useful tuneable light source. Employing this doped fibre in an optical cavity as the lasing medium, along with some tuning element, results in a continuously tuneable laser source over its broad gain profile. In fact, a tuneable erbium-doped fibre with an external grating was reported by Reekie et al. [104] in 1986. Since then several laser configurations have been demonstrated with two or more intracavity gratings [105–109].

A simple Bragg grating tuneable Er-doped fibre laser was demonstrated, where a broadband Bragg mirror and a narrow Bragg grating served as the high reflector and the output coupler, respectively [110]. The broadband mirror was constructed from a series of Bragg gratings resulting in the broadband reflector with a bandwidth of approximately 4 nm. It should be noted that with today's advancements in photosensitivity and writing techniques such a broadband mirror may have any shape and bandwidth desired. The fibre laser consisted of a two-meter long erbium-doped fibre with Bragg gratings at each end (broadband and narrowband) providing

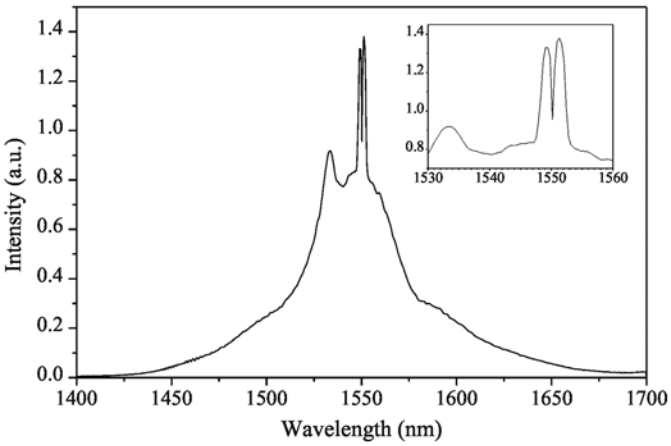

Fig. 5.42. Broadband fluorescence of an erbium-doped fibre laser. Broadband peak at 1550 nm due to broadband Bragg grating, notch within peak corresponding to Bragg grating (after [110])

feedback to the laser cavity. The output coupler to the fibre laser cavity was a single grating with approximately 80% reflectivity and 0.12 nm linewidth. Figure 5.42 shows the broadband fluorescence obtained from the Er-doped fibre laser system before lasing threshold is reached. The spectrum is the characteristic broadband gain profile from an erbium-doped fibre spanning a range of several tens of nanometres, namely between 1.45 and 1.65 μm. Superimposed on the gain profile is a broadband peak at 1550 nm corresponding to the reflection of the fluorescence from the broadband Bragg mirror and within this peak there is a notch at 1550 nm corresponding to the narrow Bragg grating. With increasing incident pump power, the losses in the fibre laser cavity are overcome and lasing begins. At pump powers just above threshold the notch due to the Bragg grating begins to grow in the positive direction and as the pump power increases further, the laser grows even stronger by depleting the broadband fluorescence.

Single frequency Er^{3+}-doped Fabry–Perot fibre lasers using fibre Bragg gratings as the end mirrors [111, 112] are emerging as an interesting alternative to distributed feedback (DFB) diode lasers for use in future optical cable television (CATV) networks and high capacity WDM communication systems [113]. They are fibre compatible, simple, scaleable to high output powers, and have low noise and kilohertz linewidth. In addition, the lasing wavelength can be determined to an accuracy of better than 0.1 nm, which is very difficult to achieve for DFB diode lasers.

Fibre lasers can operate in a single frequency mode provided that the grating bandwidth is kept below the separation between the axial mode spacings. Furthermore, it is necessary to keep the erbium concentration low enough (a few 100 ppm) to reduce ion-pair quenching, which causes a reduction in the quantum efficiency and in addition may lead to strong self-pulsation of the laser [112, 113]. The combination of these practical limits implies that the pump absorption of an erbium-doped fibre system can be as low as a few percent resulting in low output lasing power. One solution to this problem is to use the residual pump power to pump an erbium-doped fibre amplifier following the fibre laser. However, in such cases the amplified spontaneous emission from the amplifier increases the output noise. Another way to overcome the problem of low pump absorption is by codoping the erbium-doped fibre with Yb^{+3}. This increases the absorption at the pump wavelength by more than two orders of magnitude and enables highly efficient operation of centimetre long lasers with relatively low Er^{3+} concentration. Kringlebotn et al. [114] reported a highly-efficient, short, robust single-frequency and linearly polarised Er^{3+}:Yb^{3+}-codoped fibre laser with fibre grating Bragg reflectors, an output power of 19 mW, and a linewidth of 300 kHz for 100 mW of 980 nm diode pump power.

One other interesting application of Bragg gratings in fibre lasers makes use of stimulated Raman scattering. The development of fibre Bragg gratings has enabled the fabrication of numerous highly reflecting elements directly in the core of germanosilicate fibres. This technology coupled with that of cladding-pumped fibre lasers has made fibre Raman lasers possible. The pump light is introduced through one set of highly reflecting fibre Bragg gratings. The cavity consists of several hundred metres to a kilometre of germanosilicate fibre. The output consists of a set of highly reflecting gratings through Raman-order n-1 and the output wavelength of Raman-order n is coupled out by means of a partially reflecting fibre grating (R~20%). The intermediate Raman Stokes orders are contained by sets of highly reflecting fibre Bragg gratings and this power is circulated until it is nearly entirely converted to the next successive Raman Stokes order [115].

5.6.3 Fibre Bragg Grating Sensors

Fibre Bragg gratings are excellent fibre optic sensing elements. They are integrated into the light guiding core of the fibre and are wavelength encoded, eliminating the problems of amplitude or intensity variations that plague many other types of fibre sensors. Due to their narrow band wavelength reflection they are also conveniently multiplexed in a fibre optic network. Fibre gratings have been embedded into composite materials for

smart structure monitoring and tested with civil structures to monitor load levels. They have also been successfully tested as acoustic sensing arrays. Applications for fibre grating sensors should also be emerging in process control and aerospace industries in the near future.

The temperature sensitivity of a Bragg grating occurs principally through the effect on the index of refraction and to a smaller extent through the expansion coefficient (Sect. 5.2.4). It is noteworthy that temperature sensitivity can be enhanced or eliminated by proper bonding to other materials. The maximum operating temperatures may be around 500 °C, however, this may depend on the fabrication condition of the Bragg grating. For example, Type II gratings may operate at higher temperatures than Type I gratings.

Strain affects the Bragg response directly through the expansion or contraction of the grating elements and through the strain optic effect. Many other physical parameters other than tension can also be measured such as pressure, flow, vibration acoustics, acceleration, electric, magnetic fields, and certain chemical effects. Therefore, fibre Bragg gratings can be thought off as generic transducer elements. There are various schemes for detecting the Bragg resonance shift, which can be very sensitive. One such scheme involves the injection of a broadband light (generated e. g. by a super-luminescent diode, an edge-emitting LED, or an erbium-doped fibre super-fluorescent source) into the fibre and determining the peak wavelength of the reflected light. Another way involves the interrogation of the Bragg grating with a laser tuned to the sensor wavelength, or by using the sensor as a tuning element in a laser cavity. Detecting small shifts in the Bragg wavelength of fibre Bragg grating sensor elements, which corresponds to changes of the sensing parameter is important. In a laboratory environment this can be accomplished using a high precision optical spectrum analyzer. In practical applications, this function must be performed using compact, low cost instrumentation. Schemes based on simple broadband optical filtering, interferometric approaches, and fibre-laser approaches allow varying degrees of resolution and dynamic range and should be suitable for most applications.

The most straightforward means for interrogating an FBG sensor is using a passive broadband illumination of the device, and several options exist for measuring the wavelength of the optical signal reflected from the Bragg grating element, for example a miniaturized spectrometer, passive optical filtering, tracking using a tuneable filter, and interferometric detection. The optical characteristics of these filtering options are as shown in Fig. 5.43. Filtering techniques based on the use of broadband filters allow the shift in the Bragg grating wavelength of the sensor element to be assessed by comparing the transmittance through the filter compared to

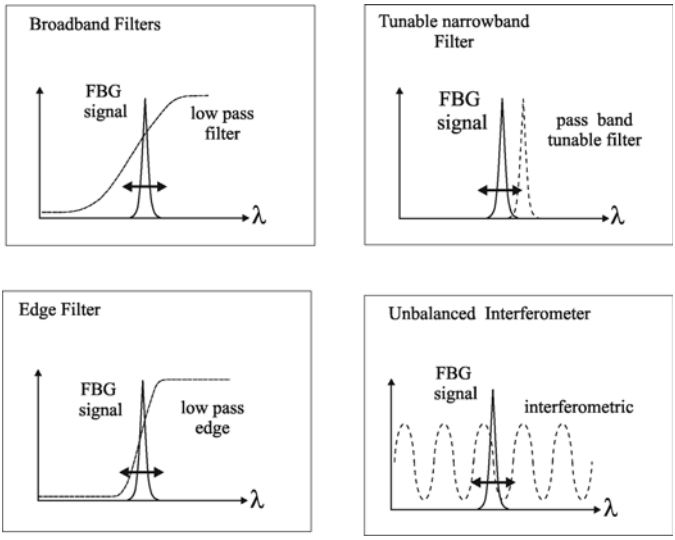

Fig. 5.43. Diagram of basic filtering function for processing fibre Bragg grating return signals

a direct 'reference' path [116]. A relatively limited sensitivity is obtained using this approach due to problems associated with the use of bulk-optic components and alignment stability. One way to improve this sensitivity is to use a fibre device with a wavelength-dependent transfer function, such as a fibre WDM coupler. Fused WDM couplers for 1550/1570 nm operation are commercially available. This coupler will provide a monotonic change in coupling ratio between two output filters for an input optical signal over the entire optical spectrum of an erbium broadband source, and has thus a suitable transfer function for wavelength discrimination over this bandwidth. An alternate means to increasing the sensitivity is to use a filter with a steeper cut-off such as an edge filter. However, this can limit the dynamic range of the system. One of the most attractive filter-based techniques for interrogating Bragg grating sensors is based on the use of a tuneable passband filter for tracking the Bragg grating signal. Examples of these types of filter include Fabry–Perot filters [117], acousto-optic filters [118], and fibre Bragg grating-based filters [119].

Tuneable Filter Interrogation

Figure 5.44 shows the configuration used to implement a tuneable filter (such as a fibre Fabry–Perot filter) to interrogate a Bragg grating sensor. The fibre Fabry–Perot can be operated in either a tracking or scanning mode for addressing a single or multiple grating element(s), respectively.

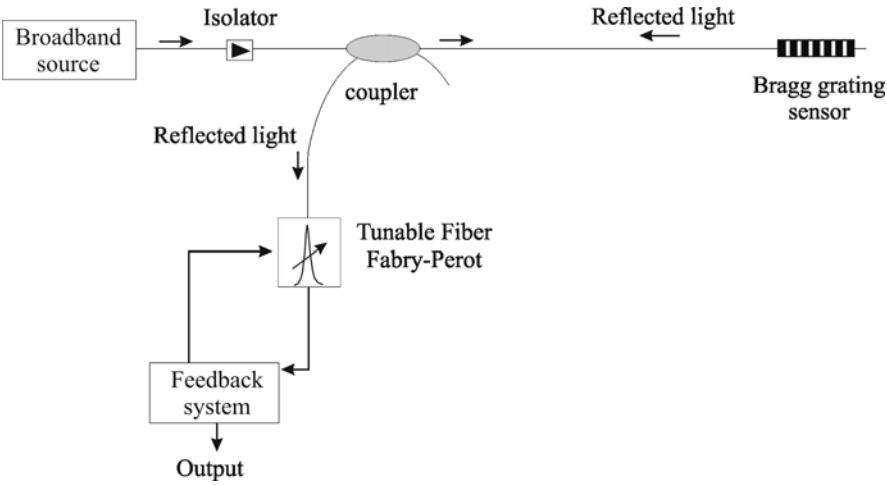

Fig. 5.44. Schematic of tuned filter-based interrogation technique for fibre Bragg grating sensors

In a single sensor configuration the Fabry–Perot filter with a bandwidth of 0.1 nm is locked to the Bragg grating reflected light using a feedback loop. This is accomplished by dithering the fibre Fabry–Perot resonance wavelength by a small amount (typically 0.01 nm) and using a feedback loop to lock to the Bragg wavelength of the sensor return signal. The fibre Fabry–Perot control voltage is a measure of the mechanical or thermal perturbation of the Bragg grating sensor.

Operating the fibre Fabry–Perot filter in a wavelength-scanning mode provides a means for addressing a number of fibre Bragg grating elements placed along a fibre path (Fig. 5.45). In this mode, the direct Bragg grating sensor spectral returns are obtained from the photodetector output. If the minimum resolvable Bragg wavelength shift that can be detected by simple scanning is insufficient, the resolution can be enhanced by dithering the Fabry–Perot filter transmission, which provides the derivative response of the spectral components in the array, i. e. a zero crossing at each of the Bragg grating centre wavelengths. This technique improves the accuracy in determining the wavelength shifts and hence the strain (or any other sensing parameter the transducer is made for).

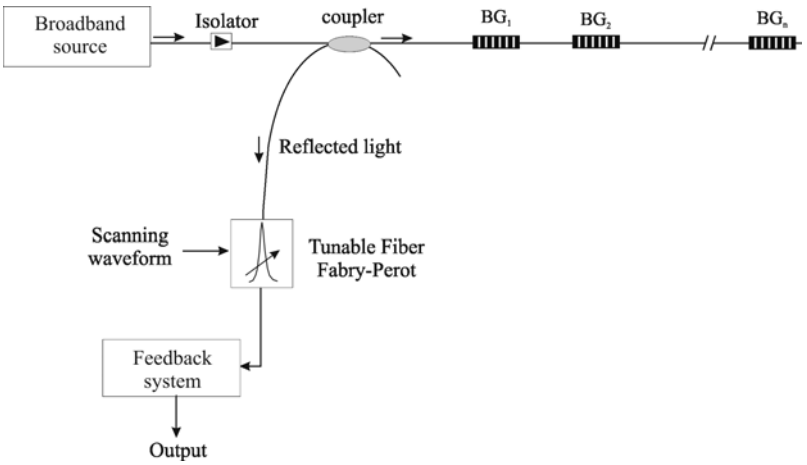

Fig. 5.45. Schematic of multiplexed fibre Bragg grating sensor array with scanning Fabry–Perot filter

Interferometric Interrogation

A sensitive technique for detecting the wavelength shifts of fibre Bragg grating sensors makes use of a fibre interferometer. The principle behind such system is shown in Fig. 5.46. Light from a broadband source is coupled along a fibre to the Bragg grating element. The wavelength component reflected back along the fibre toward the source is tapped off and fed

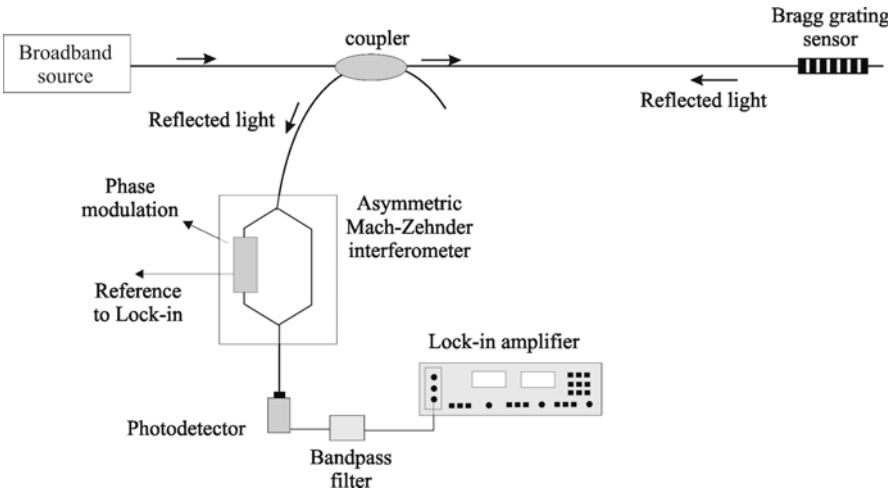

Fig. 5.46. Schematic of interferometer interrogation technique for fibre Bragg grating sensors

to unbalance the Mach–Zehnder interferometer. In effect, this light becomes the light source into the interferometer, and wavelength shifts induced by perturbation of the Bragg grating sensor resemble a wavelength-modulated source. The unbalanced interferometer behaves as a spectral filter with a raised cosine transfer function. The wavelength dependence at the interferometer output can be expressed as

$$I(\lambda_B) = A\left[1 + k\cos\left(\frac{2\pi n_{eff} d}{\lambda_B} + \phi\right)\right] \tag{5.33}$$

where A is proportional to the input intensity and system losses, d is the length imbalance between the fibre arms, n_{eff} is the effective index of the core, λ_B is the wavelength of the return light from the grating sensor, and ϕ is a bias phase offset of the Mach–Zehnder interferometer. Pseudoheterodyne phase modulation is used to generate two quadrature signals with a 90°-phase shift with respect to each other, thus providing directional information. Wavelength shifts are tracked using a phase demodulation system developed for interferometric fibre optic sensors. In practical applications, a reference wavelength source is used to provide low frequency drift compensation. Strain resolution as low as 0.6 nε/Hz$^{-0.5}$ at 500 Hz have been reported [120].

Active Laser Interrogation

In active interrogation the fibre Bragg grating sensor is used as an optical feedback element of an optical laser cavity [121]. Compared to the passive broadband base system, forming a fibre Bragg laser sensor generally provides stronger optical signals and has thus the potential to provide improved signal to noise performance. The basic concept is shown in Fig. 5.47. The laser cavity is formed between the mirror and the fibre Bragg grating element, which may be located at some sensing point. A gain section within the cavity can be provided via a semiconductor or doped fibre (such as the erbium-doped fibre). Once the laser gain is greater than unity, the fibre laser will lase at the wavelength determined by the fibre Bragg grating wavelength. As the Bragg grating changes its periodicity due to strain or temperature, the lasing wavelength will also shift. Reading of the laser wavelength using filtering, tracking filters or interferometric techniques can then be used to determine induced shifts. This laser sensor configuration is, however, limited to a single fibre Bragg grating element. A means to increase the number of Bragg gratings that can be addressed is to incorporate an additional tuning element within the cavity,

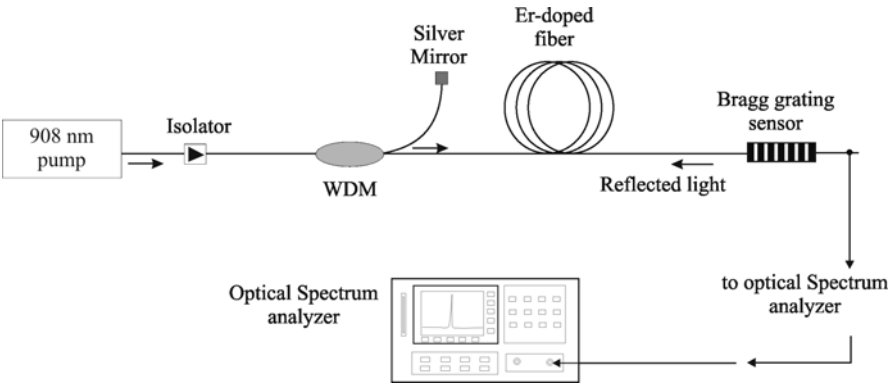

Fig. 5.47. Schematic of fibre laser sensor configuration with fibre Bragg grating elements

which selectively optimises the gain at certain wavelengths. In this way, a number of fibre Bragg gratings, each operating at a nominally different wavelength, can be addressed in a sequential manner to form a quasi-distributed fibre laser sensor. By tuning a wavelength selective filter located within the laser cavity over the gain bandwidth the laser selectively lases at each of the Bragg wavelengths of the sensors. Thus strain induced shifts in the Bragg wavelengths of the sensors are detected by the shift in the lasing wavelengths of the system.

An alternative multiplexed fibre laser sensor is based on a single element fibre laser sensor utilizing wavelength division multiplexing. Theoretically, since erbium is a homogeneously broadened medium it will support only one lasing line simultaneously. To produce several laser lines within a single length of optical fibre, a section of erbium-doped fibre is placed between the successive Bragg gratings. With sufficient pump power and enough separation between the Bragg grating centre wavelengths, a multiplexed fibre laser sensor is possible. The maximum number of sensors utilized would depend on the total pump power, the required dynamic range, and finally the gain profile of the active medium. A schematic configuration of the serially multiplexed Bragg grating fibre laser is shown in Fig. 5.48. One of the drawbacks in such a serial multiplexed configuration is that the cavities are coupled, so their respective gains are not independent. In fact, gain coupling is a common effect in such systems.

At the cost of adding more elements in a fibre laser sensor system, an alternative is to multiplex the fibre laser sensor in a parallel configuration. In essence, this system incorporates several single fibre lasers, one for each fibre Bragg grating.

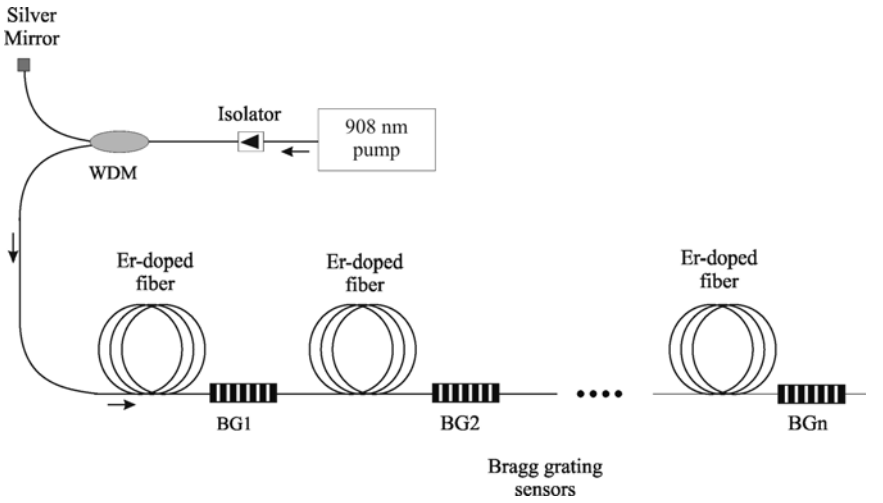

Fig. 5.48. Schematic configuration of serially multiplexed Bragg grating fibre laser

Simultaneous Measurements of Strain and Temperature

Although Bragg gratings are well suited for measuring strain and temperature in a structure, one of the drawbacks is the actual separation of the temperature from the strain component (Sect. 5.2.4). This complicates the Bragg grating application as a strain or a temperature gauge. In the case of a single measurement of the Bragg wavelength shift it is impossible to differentiate between the effects of changes in strain and temperature. Various schemes for discriminating between these effects have been developed. These include the use of a second grating element contained within a different material and placed in series with the first grating element [122] and the use of a pair of fibre gratings surface-mounted on opposite surfaces of a bent mechanical structure [123]. However, these methods have limitations when it is required to interrogate the wavelength of a large number of fibre gratings. Techniques such as measuring two different wavelengths, two different optical or grating modes have been employed [18]. In another scheme two superimposed fibre gratings with different Bragg wavelengths (850 nm and 1300 nm) have been used to simultaneously measure strain and temperature (Fig. 5.49). The change in the Bragg wavelength of the fibre grating due to a combination of strain and temperature can be expressed as

$$\Delta\lambda_B(\varepsilon,\lambda) = \Psi_\varepsilon \Delta\varepsilon + \Psi_T \Delta T \tag{5.34}$$

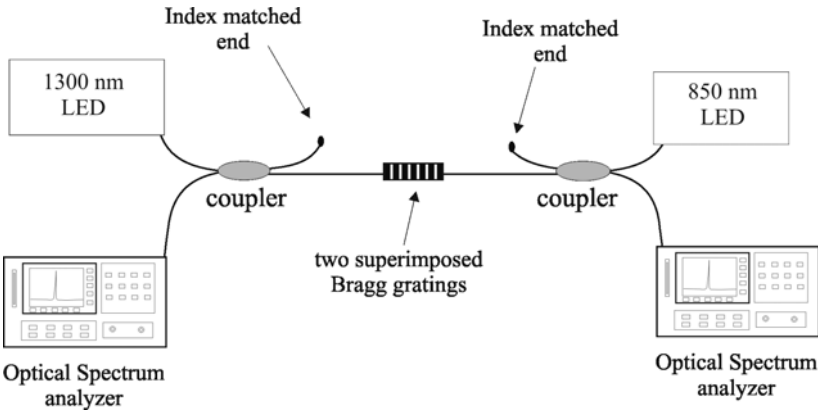

Fig. 5.49. Schematic diagram for simultaneous measurement of strain and temperature using two superimposed Bragg gratings at 1300 nm and 850 nm

In the case of two Bragg gratings with different wavelengths (referred to as 1 and 2) the following relation holds:

$$\begin{bmatrix} \Delta\lambda_{B_1} \\ \Delta\lambda_{B_2} \end{bmatrix} = \begin{bmatrix} \Psi_{\varepsilon 1} & \Psi_{T1} \\ \Psi_{\varepsilon 2} & \Psi_{T2} \end{bmatrix} \begin{bmatrix} \Delta\varepsilon \\ \Delta T \end{bmatrix} \tag{5.35}$$

The elements of the Ψ-matrix can be determined experimentally by separately measuring the Bragg wavelength changes with strain and temperature. Once Ψ is known, changes in both strain and temperature can be determined using the inverse of the above equation. The measured values of Ψ obtained in Ref. 124 (for the fibre used in that investigation) were

$$\begin{aligned} \Psi_{\varepsilon 1} &= 0.96 \pm 6.5\ x10^{-3}\,\text{pm}/\mu\text{strain} \\ \Psi_{\varepsilon 2} &= 0.59 \pm 3.4\ x10^{-3}\,\text{pm}/\mu\text{strain} \\ \Psi_{T1} &= 8.72 \pm 7.7\ x10^{-2}\,\text{pm}/\,^{0}\text{C} \\ \Psi_{T2} &= 6.30 \pm 3.7\ x10^{-2}\,\text{pm}/\,^{0}\text{C} \end{aligned} \tag{5.36}$$

where $\text{pm} = 1 \times 10^{-12}\text{m}$. If the inverse matrix is used, strain and temperature may be obtained from the two wavelength shifts. However, a drawback of this approach is the disparate wavelengths that require the use of expensive multiplexing schemes. Furthermore, the actual temperature and strain coefficients are fixed by the wavelength difference.

Recent developments have led to ways of tailoring the temperature and strain coefficients of fibre Bragg gratings (Type I and IA) by influencing the photosensitivity pre-sensitisation of the host optical fibre. Controlling the level of hydrogen saturation via hot and cold hydrogenation, can produce

gratings with tailored thermal and strain coefficients, resulting in a significant improvement in the matrix condition number, which impacts the ability to recover accurate temperature and strain data. Kalli et al. [24] designed a Type I-IA dual grating sensor that accurately decoupled temperature and strain. The key advantages of this scheme were the utilisation of two Bragg gratings having good wavelength proximity thereby avoiding costly multiplexing schemes, quick and efficient inscription using a single phase mask, common annealing cycles, and the precise placement of sensors located in a compact sensor head.

5.6.4 Aerospace Applications

The aerospace industry is a potentially important user of optical fibres, particularly for data links and fibre optic sensors. Although research projects have shown that optical fibre sensors can operate within tolerances prescribed for applications in aircraft, they are still considered an immature technology. To date efforts are directed towards the sensor development for harsh environments unsuitable for conventional electro-mechanical sensors, taking advantage of radiation resistance and EMI immunity. Increases in sensor reliability, ease of installation and maintenance with little training and without special handling are demanded, ideally leading to the so-called “fit and forget” systems.

Sensing strategies for aerospace applications broadly follow the same directions. The most important requirements are to have passive, low weight and ideally common sensors that may be multiplexed over optical links. By carefully defining sensor requirements it may be possible to specify a range of optical sensors, satisfying the majority of avionics applications, that are either interchangeable or use at least common interrogation instrumentation. Currently, many sensor types perform similar functions without being interchangeable. The Bragg grating sensor solves one of the major drawbacks of optical fibre sensors: the lack of a standard demodulation approach, while maintaining a completely passive network. The largest class of sensors measures the position of flight control elements such as landing gear status, flap and rudder position and so forth. When taking into account high levels of system redundancy well in excess of 100 sensors are employed, therefore size and weight savings become critical.

5.6.5 Applications to Civil Engineering

There is growing concern over the state of civil infrastructure in both the US and Europe. It is essential that mechanical loading be measured for

maintaining bridges, dams, tunnels, buildings and sport stadiums. By measuring the distributed strain in buildings one can predict the nature and grade of local loads, for example after an earthquake, whereas the mechanical health of bridges is increasingly under scrutiny, as old structures are often excessively loaded leading to a real possibility of increased structural failure rates. In fact, a 1996 US Department of Transportation survey estimates that 40% of all bridges in the United States are seriously deteriorated. There is concern with 50-year old railroad bridges in the US as regulatory limits on railcar loads are relaxed.

The current inspection routine depends on periodic visual inspection. The use of modern optic-based sensors can lead to real time measurements, monitoring the formation and growth of defects and optical fibre sensors allow for data to be transmitted over long distances to a central monitoring location. The advantage of optical fibres is that they may either be attached to an existing structure or embedded into concrete decks and supports prior to pouring, thereby monitoring the curing cycle and the condition of the structure during its serviceable lifetime. One of the most important applications of Bragg gratings as sensors is for "smart structures" where the grating is embedded directly into the structure to monitor its strain distribution, however, for error-free, quasi-static strain measurement temperature compensation of thermal fluctuations is required. This could lead to structures that are self-monitoring or even self-scheduling their maintenance and repair through the combination of optical fibre sensors and artificial intelligence with material science and structural engineering. Several types of fibre optic sensor are capable of sensing structural strain, for example, the intrinsic and extrinsic fibre Fabry–Perot sensor. Lee et al. [125] have used a multiplexed array of 16 fibre Fabry–Perot sensors to monitor strain on the Union Pacific Bridge that crosses the Brazos River at Waco, Texas. The fibre sensors are located at fatigue critical points for measuring dynamic loads induced by trains crossing the bridge, and the recorded data correlate well with those recovered by resistive strain gauges. Nevertheless, the general consensus is that fibre Bragg gratings are presently the most promising and widely used candidates for smart structures. The instrumentation for multiplexing large grating sensor arrays can be the same, offering a potentially low cost solution for monitoring structural strain. As the wavelength shift with strain is linear and with zero offset, long-term measurements are possible and because the measurement can be interrupt-immune one can avoid perpetual monitoring of a structure, performing periodic measurements when necessary.

References

1. A. Othonos and K. Kalli: *Fiber Bragg Gratings: Fundamentals and Applications in Telecommunications and Sensing* (Artech House, Boston, London, 1999)
2. I. Bennion, J. A. R. Williams, L. Zhang, K. Sugden, and N. J. Doran: "UV-written in-fiber Bragg gratings," Opt. and Quantum Electron. **28**, 93–135 (1996)
3. A. Othonos: "Fiber Bragg gratings," Review of Scientific Instruments **68**, 4309–4341 (1997)
4. B. J. Eggleton, A. Ahuja, P. S. Westbrook, J. A. Rogers, P. Kuo, T. N. Nielsen, and B. Mikkelsen: "Integrated tunable fiber gratings for dispersion management in high-bit rate systems," J. Lightwave Technol. **18**, 1418–1432 (2000)
5. R. I. Laming, W. H. Loh, X. Gu, M. N. Zervas, M. J. Cole, and A. D. Ellis: "Dispersion compensation with chirped fiber Bragg grating to 400 km at 10 Gbit/s in nondispersion-shifted fiber," *Opt. Fiber Commun. Conf.* (OFC'96), Techn. Digest, (San Jose, CA, USA, 1996), Vol. **2**, 203–204 (1996)
6. J. F. Brennan III, M. R. Matthews, W. V. Dower, D. J. Treadwell, W. Wang, J. Porque, and X. Fan: "Dispersion correction with a robust fiber grating over the full C-band at 10-Gb/s rates with < 0.3-dB power penalties," IEEE Photon. Technol. Lett. **15**, 1722–1724 (2003)
7. X. Chen, X. Xu, M. Zhou, D. Jiang, X. Li, J. Feng, and S. Xie: "Tunable dispersion compensation in a 10 Gb/s optical transmission system by employing a novel tunable dispersion compensator," IEEE Photon. Technol. Lett. **16**, 188–190 (2004)
8. K.-M. Feng, J.-X. Cai, V. Grubsky, D. S. Starodubov, M. I. Hayee, S. Lee, X. Jiang, A. E. Willner, and J. Feinberg: "Dynamic dispersion compensation in a 10 Gbit/s optical system using a voltage controlled tuned nonlinearly chirped fiber Bragg grating," IEEE Photon. Technol. Lett. **11**, 373–375 (1999)
9. J. Lauzon, S. Thibault, J. Martin, and F. Ouellette: "Implementation and characterization of fiber Bragg gratings linearly chirped by temperature gradient," Opt. Lett. **19**, 2027–2029 (1994)
10. P. C. Hill and B. J. Eggleton: "Strain gradient chirp of fiber Bragg grating," Electron. Lett. **30**, 1172–1174 (1994)
11. M. Pacheco, A. Medez, L. A. Zenteni, and F. Mendoz–Santoyo: "Chirping optical fiber Bragg gratings using tapered-thickness piezo-electric ceramic," Electron. Lett. **34**, 2348–2350 (1998)
12. M. M. Ohn, A. T. Alavie, R. Maaskant, M. G. Xu, F. Bilodeau, and K. O. Hill: "Dispersion variable fiber grating using a piezoelectric stack," Electron. Lett. **32**, 2000–2001 (1996)
13. P. I. Reyes, N. Litchinitser, M. Sumetsky, and P. S. Westbrook: "160-Gb/s tunable dispersion slope compensator using a chirped fiber Bragg grating and a quadratic heater," IEEE Photon. Technol. Lett. **17**, 831–833 (2005)
14. D. K. W. Lam and B. K. Garside: "Characterization of single-mode optical fiber filters," Appl. Opt. **20**, 440–445 (1981)
15. P.St. J. Russell, J. L. Archambault, and L. Reekie: "Fiber gratings," Physics World, October 1993 issue, 41–46 (1993)

16. G. Meltz and W. W. Morey: "Bragg grating formation and germanosilicate fiber photosensitivity," International Workshop on Photoinduced Self-Organization Effects in Optical Fiber, Quebec City, Quebec, May 10–11, *Proc. SPIE* **1516**, 185–199 (1991)
17. K. O. Hill and G. Meltz: "Fiber Bragg grating technology fundamentals and overview," J. Lightwave Technol. **15**, 1263–1276 (1997)
18. G. P. Brady, K. Kalli, D. J. Webb, L. Reekie, J. L. Archambault, and D. A. Jackson: "Simultaneous measurement of strain and temperature using the first- and second-order diffraction wavelengths of Bragg gratings," IEE Proceed. Optoelectron. **144**, 156–161 (1997)
19. E. Delevaque, S. Boj, J. F. Bayon, H. Poignant, J. Lemellot, and M. Monerie: "Optical fibre design for strong gratings photoimprinting with radiation mode suppression," *Opt. Fiber Commun. Conf.* (OFC'95), Techn. Digest (San Diego, CA, USA), postdeadline paper PD5 (1995)
20. H. Patrick and S. L. Gilbert: "Growth of Bragg gratings produced by continuous-wave ultraviolet light in optical fiber," Opt. Lett. **18**, 1484–1486 (1993)
21. Y. Liu, J. A. R. Williams, L. Zhang, and I. Bennion: "Abnormal spectral evolution of fibre Bragg gratings in hydrogenated fibres," Opt. Lett. **27**, 586–588 (2002)
22. A. G. Simpson, K. Kalli, K. Zhou, L. Zhang, and I. Bennion: "Formation of type IA fibre Bragg gratings in germanosilicate optical fibre," Electron. Lett. **40**, 163–164 (2004)
23. A. G. Simpson, K. Kalli, L. Zhang, K. Zhou, and I. Bennion: "Abnormal photosensitivity effects and the formation of type IA FBGs," *Conf. Bragg Gratings, Photosensitivity and Poling in Glass Waveguides* (BGPP), Techn. Digest (Monterey, CA, USA) paper MD31 (2003)
24. K. Kalli, A. G. Simpson, K. Zhou, L. Zhang, and I. Bennion: "Tailoring the temperature and strain coefficients of type I and type IA dual grating sensors – the impact of hydrogenation conditions," Measurement Science and Technology **17**, 949–954 (2006)
25. A. G. Simpson, K. Kalli, K. Zhou, L. Zhang, and I. Bennion: "An idealised method for the fabrication of temperature invariant IA-I strain sensors," postdeadline session, OFS-16 Nara, Japan, PD4 (2003)
26. K. Kalli, H. Dobb, A. G. Simpson, M. Komodromos, D. J. Webb, and I. Bennion: "Annealing and temperature coefficient study of type IA fibre Bragg gratings inscribed under strain and no strain - implications to optical fibre component reliability," *Proc. SPIE* **6193**, Reliability of Optical Fiber Components, Devices, Systems, and Networks III, 119–130 (2006)
27. I. Riant and F. Haller: "Study of the photosensitivity at 193 nm and comparison with photosensitivity at 240 nm influence of fiber tension: type IIA aging," J. Lightwave Technol. **15**, 1464–1469 (1997)
28. J. L. Archambault, L. Reekie, and P.St. J. Russell: "High reflectivity and narrow bandwidth fibre gratings written by single excimer pulse," Electron. Lett. **29**, 28–29 (1993)
29. A. Yariv: "Coupled-mode theory for guided-wave optics," IEEE J. Quantum Electron. **QE-9**, 919–933 (1973)

30. M. Yamada and K. Sakuda: "Analysis of almost-periodic distributed feedback slab waveguide via a fundamental matrix approach," Appl. Opt. **26**, 3474–3478 (1987)
31. K. O. Hill, S. Theriault, B. Malo, F. Bilodeau, T. Kitagawa, D. C. Johnson, J. Albert, K. Takiguchi, T. Kataoka, and K. Hagimoto: "Chirped in-fiber Bragg grating dispersion compensators: Linearization of the dispersion characteristic and demonstration of dispersion compensation in a 100 km, 10 Gbit/s optical fiber link," Electron. Lett. **30**, 1755–1756 (1994)
32. V. Mizrahi and J. E. Sipe: "Optical properties of photosensitive fiber phase gratings," J. Lightwave Technol. **11**, 1513–1517 (1993)
33. J. Albert, K. O. Hill, B. Malo, S. Theriault, F. Bilodeau, D. C. Johnson, and L. E. Erickson: "Apodisation of the spectral response of fiber Bragg gratings using a phase mask with variable diffraction efficiency," Electron. Lett. **31**, 222 – 223 (1995)
34. B. Malo, S. Theriault, D. C. Johnson, F. Bilodeau, J. Albert, and K. O. Hill: "Apodised in-fiber Bragg grating reflectors photoimprinted using a phase mask," Electron. Lett. **31**, 223–225 (1995)
35. R. Kashyap, A. Swanton, and D. J. Armes: "Simple technique for apodising chirped and unchirped fiber Bragg gratings," Electron. Lett. **32**, 1226 – 1228 (1996)
36. K. O. Hill, F. Bilodeau, B. Malo, T. Kitagawa, S. Theriault, C. Johnson, J. Albert, and K. Takiguchi: "Aperiodic in-fiber Bragg gratings for optical fiber dispersion compensation," *Opt. Fiber Commun. Conf.*(OFC'94), Techn. Digest (San José, CA, USA), post deadline paper PF-77 (1994)
37. K. O. Hill, F. Bilodeau, B. Malo, and D. C. Johnson: "Birefringent photosensitivity in monomode optical fibre: application to external writing of rocking filters," Electron. Lett. **27**, 1548–1550 (1991)
38. K. O. Hill, Y. Fujii, D. C. Johnson, and B. S. Kawasaki: "Photosensitivity in optical fiber waveguides: Application to reflection filter fabrication," Appl. Phys. Lett. **32**, 647–649 (1978)
39. B. S. Kawasaki, K. O. Hill, D. C. Johnson, and Y. Fujii: "Narrow-band Bragg reflectors in optical fibers," Opt. Lett. **3**, 66–68 (1978)
40. G. Meltz, W. W. Morey, and W. H. Glenn: "Formation of Bragg gratings in optical fibers by a transverse holographic method," Opt. Lett. **14**, 823–825 (1989)
41. M. L. Dockney, J. W. James, and R. P. Tatam: "Fiber Bragg grating fabricated using a wavelength tuneable source and a phase-mask based interferometer," Meas. Sci. Technol. **7**, 445 (1996)
42. R. Kashyap, J. R. Armitage, R. Wyatt, S. T. Davey, and D. L. Williams: "All-fiber narrow band reflection grating at 1500 nm," Electron. Lett. **26**, 730–732 (1990)
43. B. J. Eggleton, P. A. Krug, and L. Poladian: "Experimental demonstration of compression of dispersed optical pulses by reflection from self-chirped optical fiber Bragg gratings," Opt. Lett. **19**, 877–880 (1994)
44. H. G. Limberger, P. Y. Fonjallaz, P. Lambelet, Ch. Zimmer, R. P. Salathe, and H. H. Gilgen: "Photosensitivity and self-organization in optical fibers and waveguides," *Proc. SPIE* **2044**, Photosensitivity and Self-Organization in Optical Fibers and Waveguides, 272–285 (1993)

45. A. Othonos and X. Lee: "Narrow linewidth excimer laser for inscribing Bragg gratings in optical fibers," Rev. Sci. Instr. **66**, 3112−3115 (1995)
46. J. Cannon and S. Lee: "Fiberoptic Product News," Laser Focus World **2**, 50−51 (1994)
47. K. O. Hill, B. Malo, F. Bilodeau, D. C. Johnson, and J. Albert: "Bragg gratings fabricated in monomode photosensitive optical fiber by UV exposure thorough a phase-mask," Appl. Phys. Lett. **62**, 1035−1037 (1993)
48. A. Othonos and X. Lee: "Novel and improved methods of writing Bragg gratings with phase-masks," IEEE Photon. Technol. Lett. **7**, 1183−1185 (1995)
49. P. E. Dyer, R. J. Farley, and R. Giedl: "Analysis and application of a 0/1 order Talbot interferometer for 193 nm laser grating formation," Optics Commun. **129**, 98−108 (1996)
50. B. Malo, K. O. Hill, F. Bilodeau, D. C. Johnson, and J. Albert: "Point-by-point fabrication of micro-Bragg gratings in photosensitive fiber using single excimer pulse refractive index modification techniques," Electron. Lett. **29**, 1668–1669 (1993)
51. K. O. Hill, B. Malo, K. A. Vineberg, F. Bilodeau, D. C. Johnson, and I. Skinner: "Efficient mode-conversion in telecommunication fiber using externally written gratings," Electron. Lett. **26**, 1270–1272 (1990)
52. www.stratosphere.com
53. S. J. Mihailov, C. W. Smelser, P. Lu, R. B. Walker, D. Grobnic, H. Ding, and J. Unruh: "Fiber Bragg gratings (FBG) made with a phase mask and 800 nm femtosecond radiation," *Opt. Fiber Commun. Conf.* (OFC'03), Techn. Digest (Atlanta, GA, USA, 2003), Vol. **3**, postdeadline paper PD30 (2003)
54. S. J. Mihailov, C. W. Smelser, D. Grobnic, R. B. Walker, P. Lu, H. Ding, and J. Unruh: "Bragg gratings written in all-SiO/sub 2/ and Ge-doped core fibers with 800-nm femtosecond radiation and a phase mask," J. Lightwave Technol. **22**, 94−100 (2004)
55. D. Grobnic, C. W. Smelser, S. J. Mihailov, R. B. Walker, and P. Lu: "Fiber Bragg gratings with suppressed cladding modes made in SMF-28 with a femtosecond IR laser and a phase mask," IEEE Photon. Technol. Lett. **16**, 1864–1866 (2004)
56. A. Martinez, M. Dubov, I. Khrushchev, and I. Bennion: "Direct writing of fibre Bragg gratings by femtosecond laser," Electron. Lett. **40**, 1170–1172 (2004)
57. A. Martinez, Y. Lai, M. Dubov, I. Khrushchev, and I. Bennion: "Vector bending sensors based on fibre Bragg gratings inscribed by infrared femtosecond laser," Electron. Lett. **41**, 472–474 (2005)
58. G. D. Marshall and M. J. Withford: "Rapid production of arbitrary fiber Bragg gratings using femtosecond laser radiation," *18th Ann. Meeting IEEE Lasers & Electro-Optics Soc.* (LEOS 2005), Techn. Digest (Sydney, Australia, 2005) 935−936 (2005)
59. D. P. Hand and P.St. J. Russell: "Single-mode fibre grating written into sagnac loop using photosensitive fibre: transmission filters," *7th Internat. Conf. Integr. Optics and Opt. Fiber Commun.* (IOOC'89), Techn. Digest (Kobe, Japan), 64 (1989)
60. K. O. Hill, D. C. Johnson, F. Bilodeau, and S. Faucher: "Narrow-bandwidth optical waveguide transmission filters: A new design concept and applications to optical fiber communications," Electron. Lett. **23**, 464–465 (1987)

61. F. Bilodeau, K. O. Hill, B. Malo, D. C. Johnson, and J. Albert: "High-return-loss narrowband all-fiber bandpass Bragg transmission filter," IEEE Photon. Technol. Lett. **6**, 80–82 (1994)
62. D. C. Johnson, K. O. Hill, F. Bilodeau, and S. Faucher: " New design concept for a narrowband wavelength-selective optical tap and combiner," Electron. Lett. **23**, 668–669 (1987)
63. A. Fielding, T. J. Cullen, and H. N. Rourke: "Compact all-fiber wavelength drop and insert filter," Electron. Lett. **30**, 2160–2161 (1994)
64. D. C. Reid, C. M. Ragdale, I. Bennion, D. J. Robbins, J. Buus, and W. J. Stewart: "Phase-shifted Moiré grating fiber resonators," Electron. Lett. **26**, 10–11 (1990)
65. S. Legoubin, E. Fertein, M. Douay, P. Bernage, P. Niay, F. Bayon, and T. Georges: "Formation of Moiré grating in core of germanosilicate fiber by transverse holographic double exposure method," Electron. Lett. **27**, 1945–1946 (1991)
66. L. Zhang, K. Sugden, I. Bennion, and A. Molony: "Wide-stopband chirped fiber moiré grating transmission filters," Electron. Lett. **31**, 477–479 (1995)
67. L. Brilland, D. Pureur, J. F. Bayon, and E. Delevaque: "Slanted gratings UV-written in photosensitive cladding fibre," Electron. Lett. **35**, 234–235 (1999)
68. K. Takahashi, M. Tamura, T. Sano, K. Saito, and H. Suganuma: "Reconfigurable optical add/drop multiplexer using passive temperature-compensated wavelength tunable fiber Bragg grating," *Opt. Fiber Commun. Conf.*(OFC'01), Techn. Digest (Anaheim, CA, USA) Vol. **3**, paper WDD93 (2001)
69. P. Yvernault, D. Méchin, E. Goyat, L. Brilland, and D. Pureur: "Fully functional optical add and drop multiplexer using twin-core fiber based Mach–Zehnder interferometer with photoimprinted fiber Bragg gratings," *Opt. Fiber Commun. Conf.* (OFC'01), Techn. Digest (Anaheim, CA, USA) Vol. **3**, paper WDD92 (2001)
70. Y.-L. Lo and C.-P. Kuo: "Packaging a fiber Bragg grating without preloading in a simple athermal bimateerial device," IEEE Trans. Adv. Packaging **25**, 50–53 (2002)
71. www.gouldfo.com
72. P. Yvernault, D. Durand, D. Méchin, M. Boitel, and D. Pureur: "Passive athermal Mach–Zehnder interferometer twin-core fiber optical add/drop multiplexer," *Proc. 27th Europ. Conf. Opt. Commun.* (ECOC'01), Amsterdam, The Netherlands, Vol. **6**, 88–89 (2001)
73. W. W. Morey: "Tuneable narrow-line bandpass filter using fiber gratings," *Opt. Fiber Commun. Conf.* (OFC'91), Techn. Digest (San Diego, CA, USA), PDP 20, 96 (1991)
74. G. P. Agrawal: *Nonlinear Fiber Optics, 3rd ed.* (Academic, New York, USA, 2001)
75. www.corning.com
76. J. A. R. Williams, I. Bennion, K. Sugden, and N. J. Doran: "Fiber dispersion compensation using a chirped in fiber Bragg grating," Electron. Lett. **30**, 985–987 (1994)
77. B. J. Eggleton, P. A. Krug, and L. Poladian: "Experimental demonstration of compression of dispersed optical pulses by reflection from self-chirped optical fiber Bragg gratings," Opt. Lett. **19**, 877–880 (1994)
78. W. Loh, M. Cole, M. Zervas, S. Barcelos, and R. Laming: "Complex grating structures with uniform phase masks based on the moving fiber-scanning beam technique," Opt. Lett. **20**, 2051– (1995)

79. L. Quetel, L. Rivoallan, M. Morvan, M. Monerie, E. Delevaque, J. Y. Guilloux, and J. F. Bayon: "Chromatic dispersion compensation by apodised Bragg gratings within controlled tapered fibers," Optical Fiber Technology **3**, 267–271 (1997)
80. M. Ibsen, M. K. Durkin, M. J. Cole, and R. I. Laming: "Sinc-sampled fiber Bragg gratings for identical multiple wavelength operation," IEEE Photon. Technol. Lett. **10**, 842–844 (1998)
81. A. V. Buryak, K. Y. Kolossovski, and D.Yu. Stepanov: "Optimization of refractive index sampling for multichannel fiber Bragg gratings," IEEE J. Quantum Electron. **39**, 91–98 (2003)
82. M. Guy, F. Trépanier, and Y. Painchaud: "Manufacturing of high-channel count dispersion compensators using complex phase mask technology," OSA Topical Meeting on Bragg Gratings, Photosensitivity and Poling in Glass Waveguides (BGPP), Monterey Bay, CA, USA, 269–271 (2003)
83. A. Othonos, X. Lee, and R. M. Measures: "Superimposed multiple Bragg gratings," Electron. Lett. **30**, 1972–1974 (1994)
84. J. Lauzon, S. Thibault, J. Martin, and F. Ouellette: "Implementation and characterization of fiber Bragg gratings linearly chirped by a temperature gradient," Opt. Lett. **19**, 2027–2029 (1994)
85. T. Komukai, T. Inui, and M. Nakazawa: "Very low group delay ripple characteristics of fibre Bragg grating with chirp induced by an S-curve bending technique," Electron. Lett. **37**, 449–451 (2001)
86. A. Mugnier, E. Goyat, P. Lesueur, and D. Pureur: "Wide tuning range and low insertion loss variation dispersion compensator," Electron. Lett. **40**, 1506–1508 (2004)
87. A. Mugnier, E. Goyat, D. Pureur, and P. Yvernault: "Tunable dispersion compensating fibre Bragg grating using pure bending of a simply supported beam," *Proc. 28th Europ. Conf. Opt. Commun.* (ECOC'02), Copenhagen, Denmark, paper 10.3.5 (2002)
88. www.teraxion.com
89. C. Scheerer, C. Glingener, G. Fischer, M. Bohn, and W. Rosenkranz: "Influence of filter group delay ripples on system performance," *Proc. 25th Europ. Conf. Opt. Commun.* (ECOC'99), Nice, France, Vol. **I**, 410–411 (1999)
90. K. Ennser, M. Ibsen, M. Durkin, M. N. Zervas, and R. Laming: "Influence of nonideal chirped fiber grating characteristics on dispersion cancellation," IEEE Photon. Technol. Lett. **10**, 1476–1478 (1998)
91. M. Derrien, D. Gauden, E. Goyat, A. Mugnier, P. Yvernault, and D. Pureur: "Wavelength-frequency analysis of dispersion compensator group delay ripples," *Opt. Fiber Commun. Conf.* (OFC'03), Techn. Digest (Atlanta, GA, USA), Vol. **1**, 34–35 (2003)
92. D. Gauden, A. Mugnier, M. Gay, L. Lablonde, F. Lahoreau, and D. Pureur: "Experimental measurement of 10 Gbit/s system power penalty spectrum created by group delay ripple of fiber Bragg grating chromatic dispersion compensator," *Proc. 29th Europ. Conf. Opt. Commun.* (ECOC'03), Rimini, Italy, 684–685 (2003)
93. M. Eiselt, C. Clausen, and R. Tkach: "Performance characterization of components with group delay fluctuations," IEEE Photon. Technol. Lett. **15**, 1076–1078 (2003)
94. S. James, X. Fan, and J. Brennan III: "Performance effect in optical communication systems caused by phase ripples of dispersive components," Appl. Opt. **43**, 5033–5036 (2004)

95. A. M. Vengsarkar, P. J. Lemaire, J. B. Judkins, V. Bhatia, T. Erdogan, and J. E. Sipe: "Long-period fiber gratings as band-rejection filters," J. Lightwave Technol. **14**, 58–65 (1996)
96. M. Guy and F. Trépanier: "Chirped fiber Bragg gratings equalize gain," *WDM Solutions*, Vol. **3**(3) 77–82 (2001)
97. H. Chotard, Y. Painchaud, A. Mailloux, M. Morin, F. Trépanier, and M. Guy: "Group delay ripple of cascaded Bragg grating gain flattening filters," IEEE Photon. Technol. Lett. **14**, 1130–1132 (2002)
98. M. Guy, F. Trépanier, A. Doyle, Y. Painchaud, and R. L. Lachance: "Novel applications of fiber Bragg grating components for next-generation WDM systems," Annales des Télécommunications **58**, 1275–1306 (2003)
99. H. Renner: "Effective-index increase, form birefringence and transition losses in UV-side-illuminated photosensitive fibers," Opt. Express **9**, 546–560 (2001)
100. K. Kalli, A. G. Simpson, K. Zhou, L. Zhang, D. Birkin, T. Ellingham, and I. Bennion: "Spectral modification of type IA fibre Bragg gratings by high power near infra-red lasers," Measurement Science and Technology **17**, 968–974 (2006)
101. A. D. Kersey, M. A. Davis, J. Patrick, M. LeBlanc, K. P. Koo, C. G. Askins, M. A. Putnam, and E. J. Friebele: "Fiber grating sensors," J. Lightwave Technol. **15**, 1442–1463 (1997)
102. D. M. Bird, J. R. Armitage, R. Kashyap, R. M. A. Fatah, and K. H. Cameron: "Narrow line semiconductor laser using fiber grating," Electron. Lett. **27**, 1115–1116 (1991)
103. P. A. Morton, V. Mizrahi, P. A. Andrekson, T. Tanbun-Ek, R. A. Logan, P. Lemaire, D. L. Coblentz, A. M. Sergent, K. W. Wecht, and P.F Sciortino, Jr.: "Mode-locked Hybrid soliton pulse source with extremely wide operating frequency range," IEEE Photon. Technol. Lett. **5**, 28–31 (1993)
104. L. Reekie, R. J. Mears, S. B. Poole, and D. N. Payne: "Tuneable single-mode fiber laser," J. Lightwave Technol. **LT-4**, 956–957 (1986)
105. G. A. Ball, W. W. Morey, and J. P. Waters: "Nd^{3+} fiber laser utilizing intra-core Bragg reflectors," Electron. Lett. **26**, 1829–1830 (1990)
106. G. A. Ball and W. H. Glenn: "Design of a single-mode linear-cavity erbium fiber laser utilizing Bragg reflector," J. Lightwave Technol. **10**, 1338–1343 (1992)
107. G. A. Ball, W. H. Glenn, W. W. Morey, and P. K. Cheo: "Modeling of short, single-frequency fiber laser in high-gain fiber," IEEE Photon. Technol. Lett. **5**, 649-651 (1993)
108. G. A. Ball, W. W. Morey, and P. K.Cheo: "Single- and multi-point fiber-laser sensors," IEEE Photon. Technol. Lett. **5**, 267–270 (1993)
109. V. Mizrahi, D. J. D. DiGiovanni, R. M. Atkins, S. G. Grubb, Y. K. Park, and J. M. P. Delavaux: "Stable single-mode erbium fiber-grating laser for digital communications," J. Lightwave Technol. **11**, 2021–2025 (1993)
110. A. Othonos, X. Lee, and D. P. Tsai: "Spectrally broadband Bragg grating mirror for an erbium-doped fiber laser," Opt. Eng. **35**, 1088–1092 (1996)
111. G. A. Ball, W. W. Morey, and W. H. Glenn: "Standing-wave monomode erbium fiber laser," IEEE Photon. Technol. Lett. **3**, 613–615 (1991)
112. J. L. Zyskind, V. Mizrahi, D. J. DiGiovanni, and J. W. Sulhoff: "Short single frequency erbium-doped fiber laser," Electron. Lett. **28**, 1385–1386 (1992)

113. J. L. Zyskind, J. W. Sulhoff, P. D. Magill, K. C. Reichmann, V. Mizrahi, and D. J. DiGiovanni: "Transmission at 2.5 Gbits/s over 654 km using an erbium-doped fiber grating laser source," Electron. Lett. **29**, 1105–1106 (1993)
114. J. T. Kringlebotn, J.-L. Archambault, L. Reekie, J. E. Townsend, G. G. Vienne, and D. N. Payne: "Highly efficient, low-noise grating-feedback Er3+:Yb3+ codoped fibre laser," Electron. Lett. **30**, 972–973 (1994)
115. G. S. Grubb: "High-power 1.48 μm cascaded Raman laser in germanosilicate fibers," *Opt. Fiber Commun. Conf.* (OFC'95), Technical Digest Series, Post-conference ed. Vol. **8**, 41–42 (1995)
116. S. M. Melle, K. Liu, and R. M. Measures: "A passive wavelength demodulation system for guided-wave Bragg grating sensors," IEEE Photon. Technol. Lett. **4**, 516–518 (1992)
117. A. D. Kersey, T. A. Berkoff, and W. W. Morey: "Multiplexed fiber Bragg grating strain-sensor system with a fiber Fabry–Perot wavelength filter," Opt. Lett. **18**, 1370–1372 (1993)
118. H. Geiger, M. G. Xu, N. C. Eaton, and J. P. Dakin: "Electronic tracking system for multiplexed fiber grating sensors," Electron. Lett. **31**, 1006–1007 (1995)
119. D. A. Jackson, A. B. Lobo Ribeiro, L. Reekie, and J. L. Archambault: "Simple multiplexing scheme for fiber-optic grating sensor network," Opt. Lett. **18**, 1192–1194 (1993)
120. A. D. Kersey, T. A. Berkoff, and W. W. Morey: "High-resolution fiber-grating based strain sensor with interferometric wavelength-shift detection," Electron. Lett. **28**, 236–238 (1992)
121. A. Othonos, A. T. Alavie, S. Melle, S. E. Karr, and R. M. Measures: "Fiber Bragg grating laser sensor," Opt. Eng. **32**, 2841–2846 (1993)
122. W. W. Morey, G. Meltz, and J. M. Weiss: "Evaluation of a fiber Bragg grating hydrostatic pressure sensor," *Proceed. Opt. Fiber Sensors Conf.* (OFS-8), Monterey, CA, USA, 1992, postdeadline paper PD-4.4 (1992)
123. M. G. Xu, J. L. Archambault, L. Reekie, and J. P. Dakin: "Thermally-compensated bending gauge using surface mounted fiber gratings," Int. J. Optoelectron. **9**, 281–283 (1994)
124. M. G. Xu, J. L. Archambault, L. Reekie, and J. P. Dakin: "Discrimination between strain and temperature effects using dual-wavelength fibre grating sensors," Electron. Lett. **30**, 1085–1087 (1994)
125. W. Lee, J. Lee, C. Henderson, H. F. Taylor, R. James, C. E. Lee, V. Swenson, W. N. Gibler, R. A. Atkins, and W. G. Gemeiner: "Railroad bridge instrumentation with fiber optic sensors," *Proceed. Opt. Fiber Sensors Conf.* (OFS-12), Williamsburg, VA, USA, 1997, 412–415 (1997)